TECHNISCHE UNIVERSITÄT MÜNCHEN

Fakultät für Medizin

Relationship between electrophysiological parameters and near infrared spectroscopy during general anesthesia

Stephanie Dorothea Klinker

Vollständiger Abdruck der von der Fakultät für Medizin der Technischen Universität München zur Erlangung des akademischen Grades einer Doktorin der Medizin genehmigten Dissertation.

Vorsitz: Prof. Dr. Gabriele Multhoff

Prüfer*innen der Dissertation:

1. Prof. Dr. Gerhard Schneider
2. Prof. Dr. Vasilis Ntziachristos

Die Dissertation wurde am 12.01.2022 bei der Technischen Universität München eingereicht und durch die Fakultät für Medizin am 11.10.2022 angenommen.

Content

Abbreviations

aaMAC	age adjusted minimum alveolar concentration
aEEG	amplitude integrated electroencephalography
AUC	area under the curve
BIS	bispectral index
BMI	body mass index
BW	bandwidth (of range electroencephalogram)
CBF	cerebral blood flow
cm^2	squared centimeter
CI	confidence interval
CPB	cardiopulmonary bypass
dB	decibel
EEG	electrencephalo-graphy / -gram / -graphic
EuroSCORE	European System for Cardiac Operative Risk Evaluation
HHb	deoxygenated hemoglobin
Hz	Hertz
IQR	interquartile ranges
kg	kilogram
LM	lower margin (of range electroencephalogram)
m^2	squared meter
MAP	mean arterial pressure

mmHg	milimeter mercury
µV	microvolt
NCT	Narcotrend
NIRS	Near Infrared Spectroscopy
O_2Hb	oxygenated hemoglobin
pEEG	processed electroencephalography
PEn	permutation entropy
POCD	post-operative cognitive deficit
PSD	power spectral density
qEEG	quantitative electroencephalography
rEEG	range electroencephalography
SD	standard deviation
SE	standard error of the estimate
SpEn	spectral entropy
UM	upper margin (of range electroencephalogram)
vs.	versus

1. Introduction

Since the middle of the last century, perioperative mortality has halved (Braz, 2009). In cardiac surgery a worldwide decline of mortality to 3.9% over the last decades required a revision of the European System for Cardiac Operative Risk Evaluation (EuroSCORE) (Nashef et al., 2012). Reasons for this favorable trend are improved patient care, better surgery and anesthesia techniques, as well as improvements in monitoring (Li, 2009). With the introduction of Near Infrared Spectroscopy (NIRS) and quantitative electroencephalography (qEEG) since the 1990ies, neuromonitoring has become a new focus of investigation to improve not only mortality rate, but also stroke rate, quality of anesthesia and outcome (Calderon-Arnulphi et al., 2007; Casati et al., 2005; Douds, Straub, Kent, Bistrick, & Sistino, 2014; Harrer et al., 2010; J. M. Murkin, 2009; Ono et al., 2012; Rubio et al., 2008; Saidi & Murkin, 2005; Scheeren, Kuizenga, Maurer, Struys, & Heringlake, 2019; Subramanian et al., 2016; Thudium, Heinze, Ellerkmann, & Hilbert, 2018; Zanatta et al., 2013). EEG-based monitoring systems may help to optimize the hypnotic level in order to prevent intraoperative awareness as well as excessively deep anesthesia (Palanca, Mashour, & Avidan, 2009; Söhle, 2014). The awareness rate is given to vary around 0.2 - 2%, and can be 10 times higher in certain disciplines such as cardiac surgery (Kertai, Whitlock, & Avidan, 2012). Reducing periods of unnecessarily deep anesthesia could reduce patient morbidity, mortality and healthcare costs (Palanca et al., 2009). However, interpretation of the raw EEG trace in general, or the assessment of calculated processed EEG (pEEG) indices in certain situations, remain difficult for the clinician. During general anesthesia distinct patterns can be observed in the EEG (Brown, 2010). Besides evaluating the hypnotic level, EEG based monitoring should help to monitor cerebral saturation (Rosenthal, 2018; Guerit, 1998; Sun, 2020; Söhle, 2014). Another technique, the NIRS, should help to detect cerebral ischemia, which again is more likely to occur during cardiac surgery. Early detection and intervention can help to reduce postoperative cognitive dysfunction, occurring in about 50% of cardiac patients, and stroke rate, occurring in 1 - 3% of cardiac patients (Ghosh, Elwell, & Smith, 2012). Regarding the NIRS technique, thresholds and algorithms for intervention have yet to be defined. Combined interpretation of information derived from both, NIRS and (processed) EEG, could make patient monitoring more reliable.

1.1. Near Infrared Spectroscopy

1.1.1. Principles of Near Infrared Spectroscopy

NIRS as a non-invasive, handable method, provides continuous information on cerebral oxygen metabolism. The following section should offer basic information about the principles and development of NIRS. The mathematical background and details can be found in appropriate literature elsewhere (Ghosh et al., 2012; Suzuki, Takasaki, Ozaki, & Kobayashi, 1999; Wolf, Ferrari, & Quaresima, 2007). Based on the measurement of infrared light transmission through tissue, the concentration of light-absorbing molecules, the so-called chromophores, can be determined with the help of the Lambert Beer Law. In 1874, first observations of decreasing red light transmission with decreasing saturation of human tissue were described (A. Moerman, 2010). Almost a century later, in 1977, Jöbsis introduced infrared monitoring of cerebral and myocardial oxygen sufficiency and circulatory parameters, which is still fundamental for today's NIRS devices (Jobsis, 1977). Traversing from the emitting to the detecting optode in an elliptic pathway, light is attenuated primarily by reflectance, scattering and absorption effects. Reflection processes, as a function of the angle of light, and scattering processes have to be assumed to be nearly constant throughout the measurement. The scattering effect depends on the regional tissue composition and decreases with increasing wavelength (Ghosh et al., 2012; Jobsis, 1977). The behavior of absorption in the near infrared light spectrum (650-950 nm) mainly depends on the concentration of chromophores as hemoglobin, bilirubin, cytochrome and water (J. M. Murkin & Arango, 2009). Consequently, changes in light transmission can be explained by changes in chromophore concentrations. To obtain information on tissue oxygen saturation, oxygenated and deoxygenated hemoglobin (O_2Hb and HHb) are the relevant chromophores. One advantage of near infrared light compared to other wavelengths is its ability to penetrate skin, skull and muscle easily in order to reach cerebral tissue noninvasively and in vivo. Most of the commercial oximeters use wavelengths between 700 – 850 nm, within which the absorption maxima of O_2Hb and HHb are maximally separated, whereas the overlap with absorption effects by water is minimal (Ghosh et al., 2012; J. M. Murkin & Arango, 2009). Another advantage of near infrared light is the decreased scattering effect compared to shorter wavelengths like ultraviolet light (Jobsis, 1977). Differential spectroscopy, or the differential pathlength factor method, is the easiest way to calculate changes in chromophore concentrations with a modified

Lambert Beer Law, integrating the pathlength and scattering factor as constant variables (Ghosh et al., 2012; Wolf et al., 2007):

$$A = \frac{I}{I^{\circ}} = \varepsilon \times c \times d \times DPF + G \qquad (1)$$

With A = light attenuation, I = incident light intensity, I° = detected light intensity, ε = absorption coefficient, c = chromophore concentration, d = source–detector distance, DPF = differential path length factor and G = scattering losses.

Another basic methodology utilized in most NIRS devices is the spatial resolution, achieved by placing detectors at different distances from the emitting electrode- in terms of cerebral monitoring each attached on the patients` forehead (figure 1). Because penetration depth of the photons is directly proportional to the source-detector-distance and amounts approximately 1/3 of it, one can measure light attenuation as a function of source-detector separation and distinguish signals from extracerebral vs. cerebral tissue. The spacing of detectors ranges from 1.5 cm to 5 cm, which allows the calculation of the tissue oxygen saturation (figure 1) at a depth of up to 1.7 cm by the photon diffusion theory (A. Moerman, 2010; J. M. Murkin & Arango, 2009; Suzuki et al., 1999).

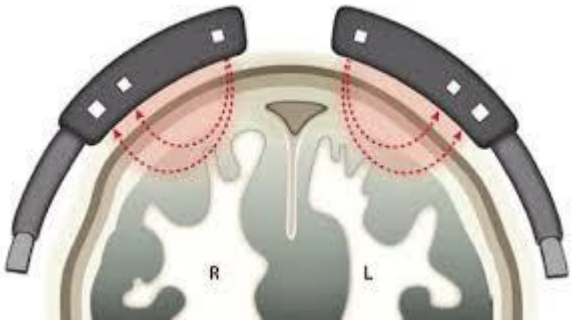

Figure 1: Schematic representation of a head with two glued-on NIRS optodes to illustrate the path of the near-infrared light (Söhle, 2014).

$$TOS\ [\%] = \frac{[O_2Hb]}{[O_2Hb + HHb]} \qquad (2)$$

With TOS = tissue oxygen saturation, O_2Hb = oxygenated hemoglobin, HHb = deoxygenated hemoglobin.

Transcutaneous NIRS reflects hemoglobin saturation of a heterogeneous tissue field and within the brain the hemoglobin distribution is assumed to be about 70% venous and 30% arterial (J. M. Murkin & Arango, 2009). According to anatomical studies, the venous component of the intracerebral vascular system ranges from 2/3 to 4/5 (Van Lieshout, Wieling, Karemaker, & Secher, 2003). However, arteriovenous proportioning can vary considerably inter- and intra-individually, which is not regarded by fixed monitors` set up (Denault André, 2007; Edmonds, 2004; J. M. Murkin & Arango, 2009).

1.1.2. Development of Near Infrared Spectroscopy

During the 1980ies NIRS found its first clinical applications in neonatology (Ghosh et al., 2012). After the first oximeter gained approval from the Food and Drug Administration in 1993 (J. M. Murkin & Arango, 2009), its use expanded to monitor the adult brain mainly in cardiac and carotid surgery (Ghosh et al., 2012). Since the 2000ies there is growing interest in NIRS guided monitoring during non-cardiac surgery as for example in critically ill patients, neuro-, trauma- and abdominal-surgery as well as during procedures in beach chair position or cardiopulmonary resuscitation (Denault André, 2007; Nielsen, 2014; Scheeren et al., 2019). Its practicability was also investigated as tool for seizure detection (Sokol, Markand, Daly, Luerssen, & Malkoff, 2000), neurovascular-coupling and functional brain monitoring (Chiarelli, Zappasodi, Di Pompeo, & Merla, 2017; Zeller, Herrmann, Ehlis, Polak, & Fallgatter, 2010), in critical care (A. Moerman, 2010) or during high altitude trekking (Hadolt I, 2003). A systematic review lists certain non-cardiac surgical procedures that provoke a reduction in NIRS determined cerebral oxygenation (Nielsen, 2014). Somatic oxygen saturation of kidney, liver, splanchnic tissue and muscle, among others, can also be observed by NIRS technology (A. Moerman, 2010; J. M. Murkin & Arango, 2009). Continuous cerebral monitoring by NIRS can help to predict outcome and mortality after traumatic brain injury or subarachnoid hemorrhage and to reduce perioperative complications (Scheeren et al., 2019). Concerning cardiac surgery, it has been estimated that NIRS is utilized in about 2/3 of pediatric and 1/4 of adult cardiopulmonary bypass (CPB) procedures in North America (J. M. Murkin, 2009) and is even considered as a standard monitor (Thudium et al., 2018). It was already suggested to integrate NIRS into standard monitoring during general anesthesia (Ghosh et al., 2012). Prior to this, it is necessary to define interpretation standards and NIRS derived treatment algorithms uniformly. Until now, the most established intervention algorithm based on NIRS monitoring was

proposed by Denault and colleagues and is provided in the Appendix (Denault André, 2007).

1.1.3. Advantages and challenges of Near Infrared Spectroscopy

The following table should summarize advantages and challenges NIRS based brain monitoring offers:

PROs (+)	CONs (-)
non-invasive, continuous (Jobsis, 1977)	heterogeneity of monitors and algorithms (Douds et al., 2014; Ghosh et al., 2012)
helpful to decrease postoperative stroke risk (Douds et al., 2014)	uncertainty of measured area (Edmonds, 2004)
interhemispheric differentiation (A. Moerman, 2010)	regional, i.e. frontal lobe (appr. 1,5 cm depth, 1 cm^3) (A. Moerman, 2010; J.M. Murkin, 2011)
helpful to decrease multiorgan morbidity and mortality (J. M. Murkin et al., 2007)	fixed arteriovenous ratio (Denault André, 2007; Edmonds, 2004)
helpful to decrease time of ventilation, hospital- and ICU stay (Douds et al., 2014)	absolute vs. relative intervention threshold (A. Moerman, 2010)
helpful to decrease number of patients with POCD (Slater et al., 2009)	false positive and negative rate (Denault André, 2007; A. Moerman, 2010)
feasible during non-pulsatile flow (Denault André, 2007)	baseline dependency for interpretation (Ghosh et al., 2012; Heringlake, 2011; J.M. Murkin, 2011)
correlates with jugular vein saturation (Edmonds, 2004; L.C., 1998; A. Moerman, Vandenplas, Bove, Wouters, & De Hert, 2013; Nagdyman et al., 2008)	influence of extracranial tissue (Edmonds, 2004; Ghosh et al., 2012)
helpful for assessment of cerebral autoregulation (Edmonds, 2004; C. Lewis, Parulkar, Bebawy, Sherwani, & Hogue, 2018; Moerman, 2016)	inter- and intraindividual optical pathlengths (Edmonds, 2004)
helpful for assessment of cerebral blood flow and volume (Ferrari, 2004)	individual tissue composition (A. Moerman, 2010)
indicator of balance between O_2 supply and demand (Zheng et al., 2013)	artefact due to motion or external light (Ghosh et al., 2012; A. Moerman, 2010)
feasible during hypothermia (down to <25°C) (J. M. Murkin, 2009; Wolf et al., 2007)	cost benefit is questionable (Intensivmedizin, 2014; Söhle, 2014; Zheng et al., 2013)

Table 1: Summary of advantages and challenges of NIRS technology.

1.2. Electroencephalography

1.2.1. Principles of Electroencephalography

Electroencephalography (EEG) is a cheap, non-invasive and continuous monitoring tool for the human brain. It offers the opportunity to reflect the simultaneous excitation of several cortical pyramidal cells by sensing voltages in the microvolt range (~20 - 150µV) (Saidi & Murkin, 2005) over the human scalp. It provides information on cerebral activity with high temporal resolution (~1 ms) (Chiarelli et al., 2017) and over a variably large area, depending on the number of electrodes. The EEG signal is a non-stationary (Asgari, Moshirvaziri, Scalzo, & Ramezan-Arab, 2018) complex signal that can contain stationary sequences (Cohen & Sances, 1977; M. Kreuzer, Kochs, Schneider, & Jordan, 2014). The recorded signal most probably presents a mixture of stochastic and deterministic signal components (Faure & Korn, 2001). It may also be considered a superimposition of oscillations at different frequencies and different amplitudes (Chiarelli et al., 2017), i.e., the EEG activity can be roughly described as the sum of different rhythms. Assuming the EEG to be a quasi-periodic oscillation, it can be characterized by frequency and amplitude. It was Hans Berger to first record human EEG successfully in 1924 and terming frequency related rhythms like the parietooccipital alpha wave rhythm (8 - 12 Hz), also known as the ´Berger's wave´. Depending on different observed frequencies, EEG can be divided into following rhythms (Chiarelli et al., 2017):

rhythm	**dominating frequency**	**note**
delta	1 – 4 Hz	during sleep in healthy population
theta	4 – 7.5 Hz	during sleep, emotional arousal and working memory
alpha	8 – 12 Hz	parietooccipital, eyes closed, awake healthy adult
beta	15 – 30 Hz	motor and sensory processing
gamma	30 – 90 Hz	in small brain areas during specific tasks e.g. multisensory integration

Table 2: Classification of electroencephalographic brain rhythm by the frequency (Chiarelli et al., 2017).

Another approach to quantify the EEG, is the amplitude integrated analysis. Amplitude-integrated EEG (aEEG) represents the peak-to-peak amplitudes of a 2 - 4 channel raw EEG, being defined as the difference between minimum and maximum voltage of one wave. During continuous monitoring, the observed voltage minima over a specific period are considered as the lower margin (LM [µV]) of the trace, whereas the maxima

represent the upper margin (UM [µV]). The difference between lower and upper margin, resulting in a bandwidth (BW [µV]), helps to capture the variability of the amplitude (O'Reilly, Navakatikyan, Filip, Greene, & Van Marter, 2012). These parameters are used to classify electrical background activity, which should provide information about the cerebral state (Del Rio et al., 2016). To classify aEEG background activity two methods have been established, addressing either the amplitude (table 3) or the voltage (table 4) pattern:

	upper margin aEEG	**lower margin aEEG**
normal amplitude	> 10 µV	> 5 µV
moderately abnormal amplitude	> 10 µV	< 5 µV
suppressed amplitude	< 10 µV	< 5 µV

Table 3: Classification of amplitude pattern based on Naqueeb and colleagues (al Naqeeb, Edwards, Cowan, & Azzopardi, 1999).

	voltage	**pattern**
Flat tracing (FT)	very low voltage < 5 µV	mainly inactive (isoelectric)
Continuous extremely low voltage (CLV)	very low voltage around 5 µV	continuous
Burst Suppression (BS)	periods of very low voltage (inactivity) intermixed with burst of higher amplitude	discontinuous
Discontinuous normal voltage (DNV)	voltage is predominantly > 5µV	discontinuous
Continuous normal voltage (CNV)	voltage 10 - 25 (- 50) µV	continuous

Table 4: Classification of voltage pattern based on Hellstrom-Westas and colleagues (Toet MC, 1999).

Still, the classical aEEG analysis is conducted using the EEG of a wide frequency range. To evaluate changes in single frequency bands, we used the computationally similar range EEG (rEEG) algorithm (O'Reilly, 2012). Within the context of this thesis, the use of the rEEG although representing a quite old method makes sense, because rEEG or aEEG were the methods of choice in a combined monitoring of EEG and NIRS (Variane, 2019; Goeral, 2017; Perez, 2015; Toet, 2006). The rEEG also calculates peak to peak voltages but without a fixed passband filter on frequencies < 2 Hz. Like aEEG analyses, rEEG also provides the three variables UM, LM and BW [µV], but for the respective

frequency range. Beyond aEEG analyses, rEEG allows to regard individual frequency bands and helps to avoid underestimation of amplitudes or disregarding the low frequencies in the raw EEG (O'Reilly et al., 2012). Hence, rEEG analyses allow to investigate the composition of the frequencies in the EEG. Figure 6 in section ´2.4.1. Range Electroencephalography´ provides a scheme of rEEG calculation from the raw EEG trace.

Beyond these basic approaches of ´EEG quantification´, there is a broad range of analytical tools today, that can be useful in clinical practice. As valid interpretation and correct technical application of the raw EEG remains one of the main difficulties, pEEG recording has become popular during the last decades (J. Bruhn, Myles, Sneyd, & Struys, 2006). The application of the Fourier transformation leads to a presentation of the EEG in the frequency domain. The amplitude spectrum is used to calculate the EEG power that can be estimated as the squared amplitude of each oscillation. Power ratios, derived from the power spectrum, can be used as trend data. So-called ´spectrograms´, or density spectral array (DSA), chromatically illustrate the weighting of specific frequency bands over the whole time of recording (Foreman B., 2012; Purdon, Sampson, Pavone, & Brown, 2015).

1.2.2. Development of Electroencephalography derived brain monitoring

Since the discovery of the EEG more than a century ago, it has found its way into many clinical disciplines, including neurology, intensive care, neonatology, and anesthesia. In the context of perioperative brain monitoring, the EEG is indicative of both, ischemia, and level of consciousness. One could observe a change from low-amplitude, high-frequency signals in awake patients to high-amplitude, low-frequency signals at deeper levels of anesthesia (Brown, 2010; Aryeh, 2018; Saidi & Murkin, 2005). Further, an electrophysiological reaction to ischemia by general slowing manifested as a decrease in amplitude of higher frequencies and an increase in amplitude of lower frequencies, has been described (C. Lewis et al., 2018; Foreman B., 2012). Generally, cerebral desaturation leads to similar EEG patterns as deepening of the anesthesia (Söhle, 2014). As mentioned above, the number of sensors varies with the aim of application, ranging from 256 for high density arrays with increased spatial resolution (Robinson et al., 2017) to frontal 2 - 4 channel EEG in long term recordings or anesthesia monitors (Chiarelli et al., 2017). Continuous EEG recording is utilized for seizure detection in the intensive care unit and can contribute to seizure and epilepsy characterization (Foreman B., 2012). During cardiac and neurological surgery, continuous EEG has frequently been

used for more than 50 years to detect reduced oxygen delivery (Foreman B., 2012; C. Lewis et al., 2018). Electrophysiological changes are closely tied to cerebral blood flow (CBF) (Foreman B., 2012) and therefore considered in vasospasm monitoring after subarachnoid hemorrhage (Muniz et al., 2016) or cerebral function assessment after cardiac arrest (Drohan et al., 2018; Friberg et al., 2013).

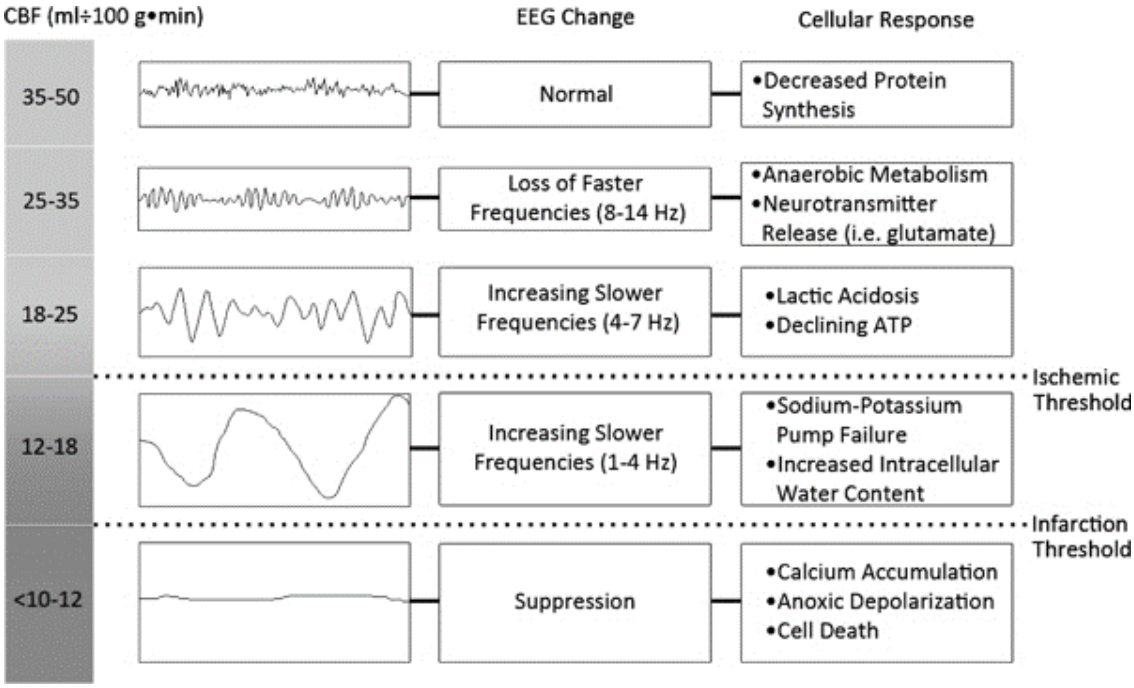

Figure 2: The relationship of Cerebral Blood Flow (CBF) to raw EEG and to cellular response based on Foreman et. al (Foreman B., 2012).

Since the 1990ies, several EEG derived monitors for state of anesthesia assessment like the Bispectral Index monitor™ (BIS, Medtronic, Minneapolis, MN), the Entropy module (GE Healthcare Technologies, Helsinki, Finland) and the Narcotrend Monitor™ (NCT, MonitorTechnik, Bad Bramstedt, Germany) have been developed. Besides analysis of the EEG in the spectral domain, each product uses different and partly proprietary algorithms, which makes comparison difficult (J. Bruhn et al., 2006). What they have in common, is the intention to translate the complex, non-linear EEG signal into a dimensionless, linear parameter in order to reflect the state of (un-)consciousness. Another proposed aim is to reflect the probability of awareness during general anesthesia, which may not have been achieved yet (Pandit & Cook, 2013). Assessing the patients' response to anesthetics may help to reduce the risk for both, unintended awareness and for excessively deep anesthesia. Preventing an inadequate level of

anesthesia can help to reduce postoperative stress disorder, myocardial infarction, stroke and cognitive dysfunction (Shepherd et al., 2013). However, the EEG is influenced by many factors, including cerebral desaturation, age, neurological disorder, body temperature and relevant comorbidities (Kaiser et al., 2020). In terms of perioperative monitoring, electrical and mechanical artifacts as well as the specific anesthetic drug influence the EEG additionally (Aryeh, 2018; Levy, 1984; Purdon, Pavone, et al., 2015; Purdon, Sampson, et al., 2015; Scheeren et al., 2019). Processed EEG monitors were primarily developed to evaluate the anesthetic level rather than to detect cerebral ischemia (Söhle, 2014). In terms of monitoring the hypnotic level of anesthesia, various task forces recommend using pEEG during total intravenous anesthesia, deep hypothermic circulatory arrest (DHCA) and of patients with greater risk for intraoperative awareness (Söhle, 2014; Michels P. et al., 2017).

For specific high-risk populations, such as elderly with greater risk of postoperative delirium, a grade ´A´ recommendation for ´depth-of-anesthesia´ monitoring has been proposed by the European Society of Anesthesiologists recently (Fahy B.G., 2017). The use of intraoperative EEG information is suggested to prevent postoperative neurocognitive disorders (Aldecoa et al., 2017; Chan et al., 2020).

Amplitude integrated EEG recording, indicative for asphyxia and correlating with findings in the raw EEG (al Naqeeb, Edwards, Cowan, & Azzopardi, 1999; Del Rio et al., 2016; Schettler, 2013), was introduced for adults in the late 1960s and established in neonatology throughout the 1980ies (de Vries & Hellstrom-Westas, 2005; Schettler, 2013). One advantage of aEEG based monitoring is its reliability during mild hypothermia (Gluckman et al., 2005; Horan, Azzopardi, Edwards, Firmin, & Field, 2007). It has been investigated for assessment of infants with encephalopathy (al Naqeeb et al., 1999; Goeral et al., 2015) or outcome and survival prediction after cardiac arrest (Drohan et al., 2018; Friberg et al., 2013). In terms of intraoperative brain monitoring, the previously mentioned pEEG monitors also regard changes in amplitude in their index calculation. However, whether a change of the calculated index is due to a change in amplitudes is not obvious. Moreover, whether the change in amplitudes is due to a change in anesthesia level, cerebral desaturation, artifacts or any other factor cannot be determined so far.

1.2.3. Advantages and challenges of Electroencephalography derived brain monitoring

The following table summarizes advantages and challenges EEG based brain monitoring offers:

PROs (+)	CONs (-)
cheap, fast, noninvasive (Chiarelli et al., 2017)	interpretation (Foreman B., 2012; C. Lewis et al., 2018; Saidi & Murkin, 2005)
high temporal resolution (Robinson et al., 2017)	hypothermia and anesthetics (Saidi & Murkin, 2005)
comparability and reproducibility due to 10-20 system (Chiarelli et al., 2017; Drohan et al., 2018)	sensor placement (Aryeh, 2018)
specific and early (Foreman B., 2012) for brain ischemia (C. Lewis et al., 2018)	attenuation by pre-existing cortical injury (C. Lewis et al., 2018)
outcome prediction after cardiac arrest (Asgari et al., 2018)	interference with electrical signals and cautery (C. Lewis et al., 2018; Schuller P.J. et al., 2015)
feasible for continuous monitoring (Foreman B., 2012)	hypothermia as a confounding factor (C. Lewis et al., 2018; Saidi & Murkin, 2005)
correlative to CBF (Foreman B., 2012; Muniz et al., 2016)	medication as a confounding factor (Aryeh, 2018; C. Lewis et al., 2018)
can be quantified (Foreman B., 2012)	proprietary algorithms in EEG based monitors (Aryeh, 2018)
comparison between different brain regions possible (Foreman B., 2012)	muscle activity as a confounding factor (C. Lewis et al., 2018)
tool for state of anesthesia assessment (C. Lewis et al., 2018; Palanca et al., 2009)	influenced by age and comorbidities (Aryeh, 2018; Matthias Kreuzer et al., 2020, Kaiser et al., 2020)
pEEG monitors easy to interpret (scale from 0 – 100)	drug-specific alterations (Scheeren et al., 2019)

Table 5: Summary of advantages and challenges of EEG derived brain monitoring.

1.3. Combined monitoring

Since many systemic parameters can influence EEG indices, they should be interpreted in conjunction with the raw EEG, possibly supported by the spectrogram as well as blood pressure, systemic oxygenation or perfusion pressure (Foreman B., 2012). NIRS and EEG technology both provide information about cerebral integrity and function and are increasingly used in the perioperative management (Scheeren et al., 2019). Both react to ischemia and can be used clinically as continuous, non-invasive, relatively cheap and handy tools. The simultaneous application of NIRS and EEG is possible, due to the lack of severe electro-optical interference (Chiarelli et al., 2017). However, ischemia and anesthesia influence the EEG in a similar way. Therefore, the EEG can only be used as an ischemia monitor if the level of anesthesia remains stable and if spontaneous electrical activity is maintained (Söhle, 2014). Equally, it may be possible that in terms of pEEG analyses, brain ischemia leads to index values outside the target range, independent from the current level of anesthesia. In certain surgical settings, such as cardiac and thoracic surgery, the patients are exposed to an increased risk of both, awareness and cerebral ischemia (Ghosh et al., 2012; J.M. Murkin, 2011; Kertai et al., 2012). For this reason, extended neuromonitoring with the addition of NIRS is performed here. Neither cerebral deoxygenation nor changes in cerebral activation can be explained monocausally. Therefore, and since brain oxygenation is probably related to brain function, it may be advantageous to interpret intraoperative EEG and NIRS measurement together (Caicedo et al., 2016). Also, in terms of autoregulation monitoring of the brain, both methods may be useful (Edmonds 2004, Moerman 2016, Lewis, Parulkar et al. 2018, Scheeren, Kuizenga et al. 2019). There are indicators that the limits of autoregulation are shifted in certain patient groups (Edmonds, 2004; Joshi et al., 2010; Ono et al., 2012). It could be helpful to re-evaluate the assumption that the oxygen supply to the brain is autoregulated and therefore not in need of monitoring during general anesthesia. The current state of research suggests that inhaled anesthetic agents can impair cerebral autoregulation in a dose-related manner (Dagal & Lam, 2009; Strebel et al., 1995). To assess autoregulation during general anesthesia, transcranial Dopplersonography has been recommended (Dagal & Lam, 2009). For selective time periods, NIRS-based autoregulation monitoring was described as more suitable than Doppler-based autoregulation monitoring (C. Lewis et al., 2018). There are already calls for multimodal monitoring (Asgari et al., 2018; Schneider, 2014; Thudium et al., 2018) and the combination of EEG and NIRS (Goeral et al., 2017; Perez et al.,

2015; Scheeren et al., 2019). An animal study indicates that aEEG reflects cerebral function consistently and accurately at different cerebral regional O_2 saturation levels (Dandan, 2008). In line with that, aEEG and NIRS have been proven to be important predictors of short-term outcome in hypothermia treated neonates, especially when combined (Goeral et al., 2017; Variane, Chock, Netto, Pietrobom, & Van Meurs, 2019). Another study supports the bilateral use of BIS and NIRS monitoring for tracking changes in CBF during carotid endarterectomy under general anesthesia (Perez et al., 2015). Hence the physiological mechanism of the link between EEG and NIRS is still unclear, more studies are required (Caicedo et al., 2016; Roche-Labarbe, Wallois, Ponchel, Kongolo, & Grebe, 2007).

1.4. Research question

Interpretation of the raw EEG and integrating this signal into standard monitoring remains one of the main difficulties for the user. The idea of using pEEG monitors to overcome this challenge, makes it difficult to differentiate between all possible influencing factors on the displayed EEG. To optimize EEG-based anesthesia monitoring, a differentiation between anesthetic and non-anesthetic related EEG changes is crucial. Hence, identifying brain saturation related changes with the help of NIRS can help to improve monitoring.

This doctoral thesis presents results from a pilot investigation regarding the relationship between NIRS signal and EEG derived parameters in 307 adult patients undergoing cardiac surgery under general anesthesia. Therefore, different relevant EEG parameters are regarded, including raw EEG and processed EEG parameters as well as monitor related indices. A combination of EEG and NIRS provides both, an electrophysiological and metabolic approach to depict brain state. To better understand how NIRS and EEG relate to each other as unaffected from certain surgical or anesthesiologic procedures as possible, the method of analysis is elaborated in different steps. The relationship between NIRS and electrophysiological parameters under general anesthesia in adults has not been investigated well yet. Eventually, these analyses could contribute to planning future prospective studies, identifying and validating brain saturation-specific changes in the EEG. The opportunity due to the large number of cases on the one hand and the limitations due to the retrospective, explorative approach on the other hand should be noted a priori. The main intention of the thesis was to identify and describe

possible associations between NIRS and EEG parameters at controlled conditions. We further investigated the influence of temperature on the EEG.

2. Material and Methods

2.1. Data recording

Intraoperative data from 439 Patients scheduled for cardiac surgery on CPB were recorded externally in the Inselspital Bern, Switzerland. The data collection was observational without intervention or randomization on anesthesiologic or surgical grounds. Patients consent and approval of the ethical committee for collecting and analyzing of biosignals was given in written form: *ClinicalTrials.gov Identifier: NCT02976584; ethics committee of the canton of Bern KEK#210/15*. Most procedures consisted of coronary artery bypass graft or valve replacement and all were listed and weighed according to EuroSCORE II (Nashef et al., 2012), which can be found in the appendix. The records include standard monitoring with electrocardiography, capnography and respiratory parameters (Primus by Draeger, Luebeck, Germany). Further, arterial oxygen saturation, arterial blood pressure with calculated mean arterial pressure (MAP) and body temperature (rectal or nasopharyngeal probe) were recorded. In terms of Neuromonitoring, bifrontal regional NIRS (NIRO [Hamamatsu Photonics, Japan] and few recordings with EQUANOX™ [Nonin Medical Inc, Plymouth, USA] or INVOS™ [Somanetics Corp, Minneapolis, USA]) with a sampling rate of 1 Hz and bifrontal regional EEG (Narcotrend monitor, Hannover, Germany) at a sampling rate of 125 Hz were recorded. NIRS and Narcotrend monitors were connected to a Philips IntelliVue MP90 anesthesia monitor (Philips Medical Systems, Eindhoven, Netherlands) with IntelliBridge modules and data were extracted using the Rugloop II software (Demed Medical, Temse, Belgium). All records were time-synchronized and marked with timepoints to label start and end of the OP, the period of aortic clamping as well as initiation and end of CPB.

2.2. Data preparation

Criteria for exclusion were non-Isoflurane general anesthesia or a combination of volatile anesthetics. Also, incomplete recordings of end-tidal gas concentration, temperature, EEG or NIRS were excluded. ´High´ risk patients and settings were defined as

undergoing a re-operation, multiple periods of extracorporal circulation, emergency intervention, intraoperative resuscitation or death, sepsis and shock. This ´high´ risk cohort was also excluded. It was s not controlled for age specifically, but for any analyses the age-adjusted minimum alveolar concentration (aaMAC) was calculated from the end-tidal Isoflurane concentration according to Nickalls and colleagues (Nickalls & Mapleson, 2003). Finally, 307 patients were selected for analyses.
Following flow chart helps to illustrate the selection of the patients for our analyses:

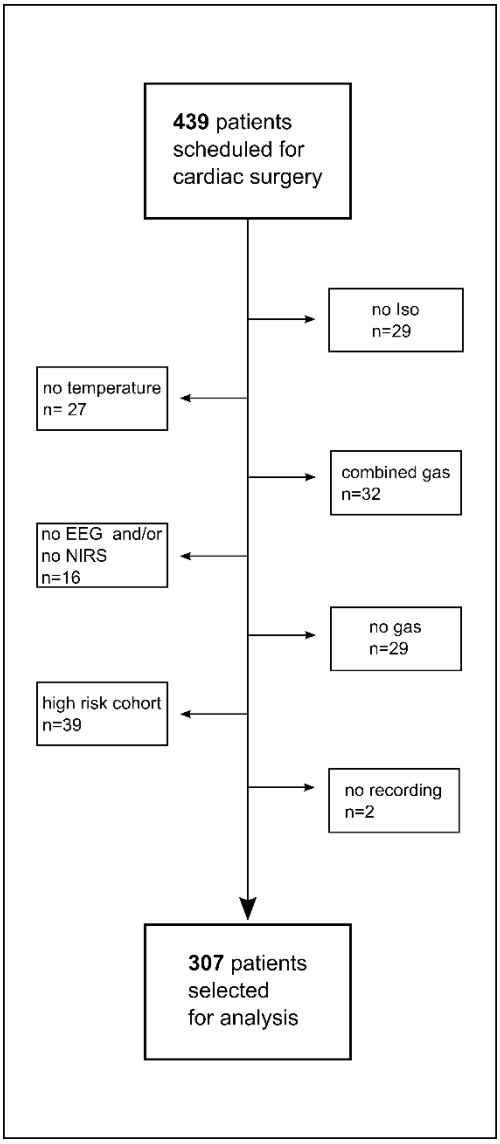

Figure 3: Flowchart of patients` selection.

2.3. Elaboration of the analysis concept

To evaluate the impact of NIRS on the EEG parameters, we decided to only include EEG parameters derived at controlled conditions such as:

- recorded before aortic cross-clamping
- at a temperature above 35°C
- with the MAP within 50 - 150 mmHg
- under general anesthesia between 0.6 and 0.8 aaMAC

because all these factors can significantly influence the EEG. The EEG can be influenced by various other factors. These can be patient related (e.g. age, BMI, ethnic, neuronal disease, muscle activity, hypoxia, diabetes / cardiac / renal comorbidities) as well as procedural related (e.g. mechanical artefact, electrocautery, anesthetic drug, deep hypothermic circulatory arrest) and are often difficult to notice (Lewis, 2018; Saidi, 2005; Scheeren, 2019; Kreuzer, 2020; Kaiser, 2020). In this retrospective approach it is even more difficult to define and exclude influencing factors on the EEG in order to investigate the relationship to the NIRS signal as precisely as possible. To control for likely influences on the EEG within our cohort, the thresholds for temperature, MAP and aaMAC were (re-) evaluated.

2.3.1. Influence of the temperature on the amplitudes of the Electroencephalography

The influence of temperature on the EEG signal was proposed long ago already (Levy, 1984). Concerning cardiac surgery with the use of CPB, a linear correlation between body temperature and peak power as well as between body temperature and peak power frequency in the high frequency band has been described for the period of rewarming (Levy, 1984). Concerning pEEG monitors, moderate hypothermia (28 - 30°C) during CPB reveals lower BIS Indices when compared to mild hypothermia (32 - 34°C) (Honan, Doherty, & Frizelle, 2006). Also the NCT index can decline with temperature (Dennhardt et al., 2018). In cardiac anesthesia, a weak but statistically significant negative correlation between BIS and mixed venous oxygen saturation was observed exclusively in hypothermic patients < 34.1°C (Stein, 2010). Amplitude integrated EEG seems to remain feasible for brain monitoring of neonates during Hypothermia down to 34 - 35°C rectal temperature (Gluckman, Wyatt et al. 2005). Within our cohort, the

proposed threshold for temperature influence on the EEG was validated before further analyses as presented in figure 4. In accordance with descriptions in the literature, EEG changes in amplitudes appeared at a body temperature of ≤ 34°C (Stein, 2010; Dennhardt, 2018).

Figure 4 illustrates pooled data pairs of simultaneously sampled rEEG (UM [µV]) and NIRS recording at a sampling rate of 1 Hz for the frequencies in the alpha (8 - 12 Hz), beta (12 - 25 Hz), delta (0.5 - 4 Hz) and theta (4 - 8 Hz) range. The period from start of recording in the operation room until aortic clamping before initiation of CPB was considered. It was controlled for the MAP to be within 50 - 150 mmHg and for the aaMAC to be within 0.6 - 0.8. The color codes for the amplitude size of the UM [µV] and visualizes a general decline of amplitudes when the patients' temperature falls below 35°C. To minimize the influence of temperature, we only included recordings during periods with the patients' temperature of > 35°C for all further analyses.

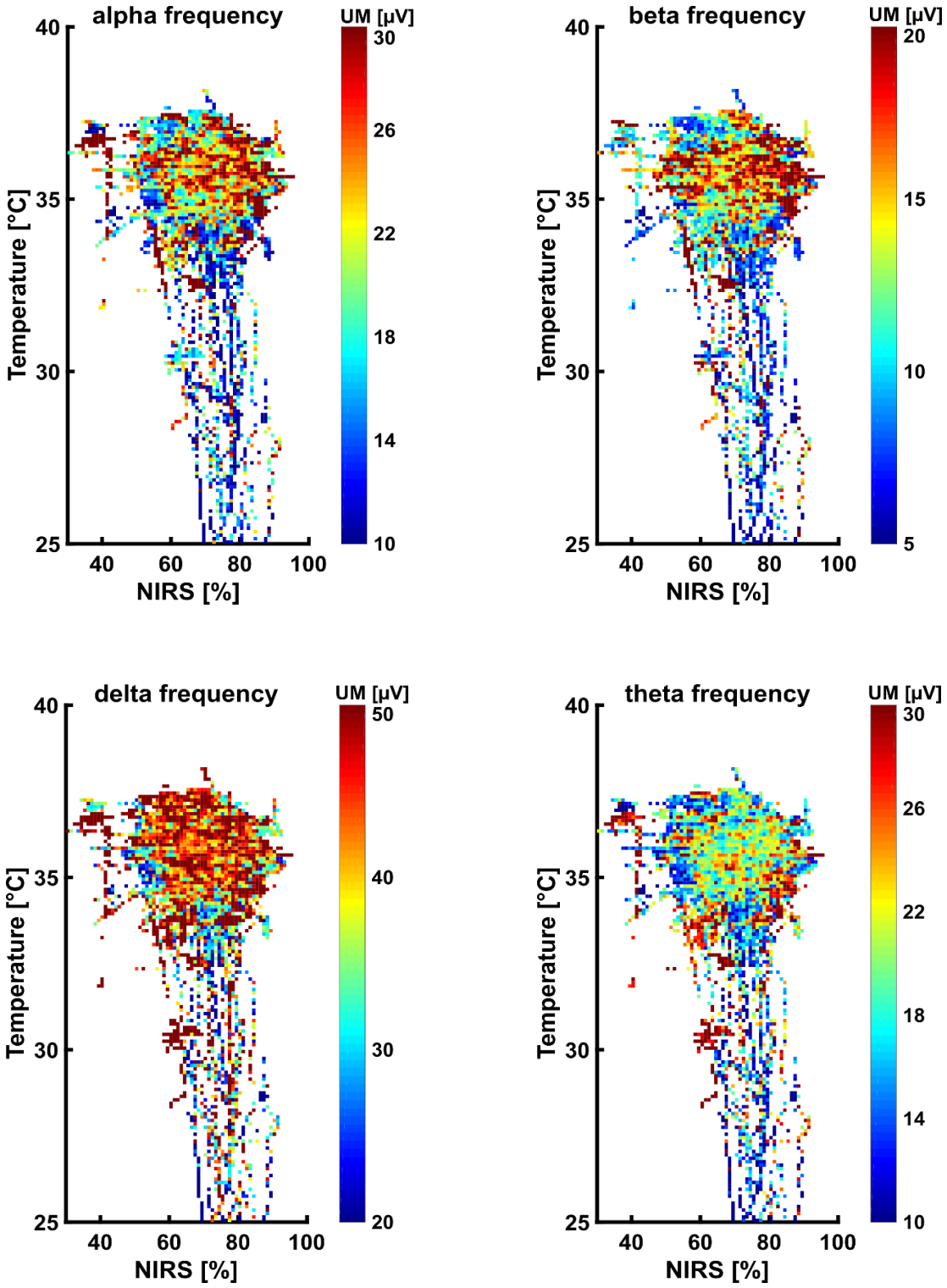

Figure 4: Influence of the body temperature on data pairs of NIRS and frontal rEEG in the alpha, beta, delta and theta frequency.

2.3.2. Influence of the mean arterial pressure on cerebral perfusion

Electrophysiological changes are closely tied to CBF (Foreman B., 2012). The principle of autoregulation states that the CBF can be maintained by cerebral vasoreactivity independent from fluctuations of the MAP within the autoregulated MAP range (Edmonds, 2004). Consequently, changes in the MAP should not extensively influence the EEG, as long as the autoregulation mechanism is intact. However, current state of research suggests that the autoregulation limits in certain patient groups deviate significantly from the mentioned range of 50 - 150 mmHg (Edmonds, 2004; Scheeren et al., 2019). For example, a shift of the lower autoregulation limit to > 66 mmHg was observed during CPB (Hori et al., 2014). Moreover, a wide range of MAP at the lower limit of autoregulation (LLA) during CPB from 40 to 90 mmHg has been described (C. Lewis et al., 2018). A study on 234 patients showed that impaired cerebral autoregulation occurred in 20% of patients during CPB (Ono et al., 2012). Intraoperative MAP values during CPB could be changed by adjusting pulsatile or non-pulsatile flow alone (Tovedal, Thelin, & Lennmyr, 2016). Vasoactive drugs could cause paradoxical changes in cerebral oxygen saturation with changes of the MAP. Notably, a paradox response of the cerebral oxygen saturation to changes of the MAP could be observed exclusively in patients with intact autoregulation (Moerman, 2016). In summary, cerebral autoregulation mechanism and CBF monitoring remain complex phenomena (Ferrari, 2004; Moerman, 2016). In a study by Murkin and colleagues, maintaining MAP above 50 mmHg was considered as ´best clinical practice´ (J. M. Murkin et al., 2007). Neither the definition of the autoregulation range nor the MAP target values should be defined by our analyses. Nevertheless, to minimize the risk of autoregulation or MAP abnormalities interfering with the NIRS or EEG signal, only the MAP range of 50 - 150 mmHg and only the period before initiation of CBP were included in the main analyses.

2.3.3. Influence of the minimum alveolar concentration on the Electroencephalography

To validate our approach and to illustrate the complex interplay of the recorded biosignals, we evaluated data from the whole observed aaMAC range in combination with pEEG and NIRS dynamics.

The pre-analyses of the whole observed aaMAC range should underline the need to concentrate only on a defined aaMAC range for more accurate analyses and validate our choice of the 0.6 - 0.8 aaMAC. First, this range seems to provide an adequate level of anesthesia for this patient group and for this surgical intervention. Second, this range provides a low risk of provoking Burst Suppression in the EEG. As a pEEG parameter for this investigation we used the NCT index which ranges from 100 (awake) to 0 (electrical silence) (Kreuer & Wilhelm, 2006). In the EEG, a deepening of anesthesia through an increased supply of the gas concentration can look similarly to cerebral desaturation. It is therefore recommended to use the EEG for cerebral ischemia detection only if the applied anesthetic gas concentration remains unchanged (Söhle, 2014). The targeted MAC can vary greatly depending on the patient population or the type of procedure. Hence, it would be interesting to know if the relation between EEG and saturation changes between either constantly high or constantly low gas concentration, and if our selected 0.6 - 0.8 aaMAC range seems adequate. This pre-analysis should help to show if the correlation between pEEG analysis, as integrated in the NCT monitor, and the NIRS changes dependent on the aaMAC. For example, if the correlation is different at a constant aaMAC of 1.6 compared to a constant aaMAC of 0.2. In our study, the risk of changes in the aaMAC interfering with the NIRS or EEG signal, should be minimized by defining limits of the included aaMAC values. Therefore, we used a linear regression model for a wide range of aaMAC values (0.2 - 1.6), to evaluate the impact of cerebral desaturation (evaluated with NIRS) on the pEEG (evaluated with NCT index).

The linear regression models for the NCT index versus NIRS (figure 5) revealed a dependence of the NCT on NIRS. All values were observed at a body temperature >35°C. One graph represents one stable aaMAC, ranging from 0.2 - 1.6 in steps of +0.1. The colorbar codes for the aaMAC range from blue (0.2) to dark red (1.6).

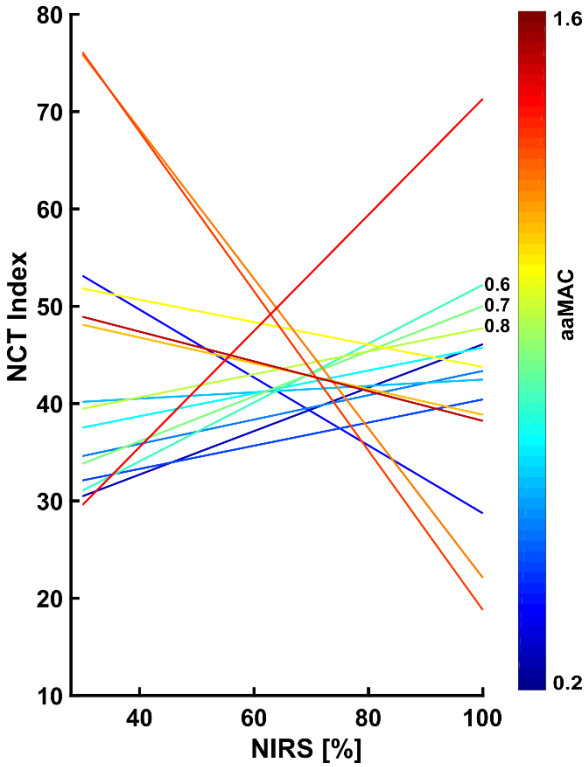

Figure 5: The influence of the aaMAC on the NCT index with included aaMAC range for the main analyses (0.6 - 0.8) explicitly listed next to their corresponding graphs.

Figure 5 illustrates that the direction of a link between NCT index and NIRS value can be reversed comparing either very high or very low aaMAC values within our cohort. For the lower aaMAC values the recorded NCT index increased as the NIRS value increased, except for one (aaMAC 0.3). Conversely, for the higher aaMAC values the NCT index decreased as the NIRS value increased, except for the aaMAC of 1.6. The fact that at the highest aaMAC concentration of 1.6 the NCT index fell as the NIRS value rose could be due to occurrence of burst suppression in the raw EEG, which was undetected by the NCT monitor. Although an examination of the monitor or the dependence of the link between index-calculation and NIRS value on the MAC would be very interesting, it was not subject of current research. Currently, figure 5 underlines the importance of limiting the included aaMAC range to 0.6 - 0.8 in terms of interpreting studies on the relation between corresponding NIRS and EEG parameters. This range also corresponds to the pronounced intraoperative target MAC for our cohort.

2.4. Processed Electroencephalography parameters

To describe possible changes caused by the saturation status, we applied a set of (processed) EEG parameters to the data. Therefore, we investigated whether the EEG parameter reacts specifically to the current cerebral saturation. For these analyses, all simultaneously occurring NIRS, EEG parameter and aaMAC values of the 307 patients were used. As mentioned above, we controlled for the temperature to be > 35°C, the MAP to be within the estimated autoregulation range of 50 - 150 mmHg and limited our analyses to the 0.6 - 0.8 aaMAC range.

2.4.1. Range Electroencephalography

Amplitude integrated EEG (aEEG) is an EEG parameter that is used in combination with NIRS already (Goeral et al., 2017). Pursuing to avoid underestimation of amplitudes or disregarding low frequencies, rEEG is a recently developed alternative to aEEG (O'Reilly, Navakatikyan et al. 2012). It is chosen for our analyses of saturation related influence on the adult brain under general anesthesia, where especially lower frequencies might be important. Analyzed raw EEG sections are divided into the alpha (8 - 12 Hz), beta (12 - 25 Hz), delta (0.5 - 4 Hz) and theta (4 - 8 Hz) frequency range for rEEG calculation. This approach aims to investigate whether specific frequencies react differently to current cerebral (de)saturation. For example, the EEG alpha frequency is described to react early on cerebral ischemia (Söhle, 2014). The alpha frequency is predominantly expressed in the frontal brain during general anesthesia and its predominance is assumed to be revealed relatively independently from age (Purdon et al., 2015).

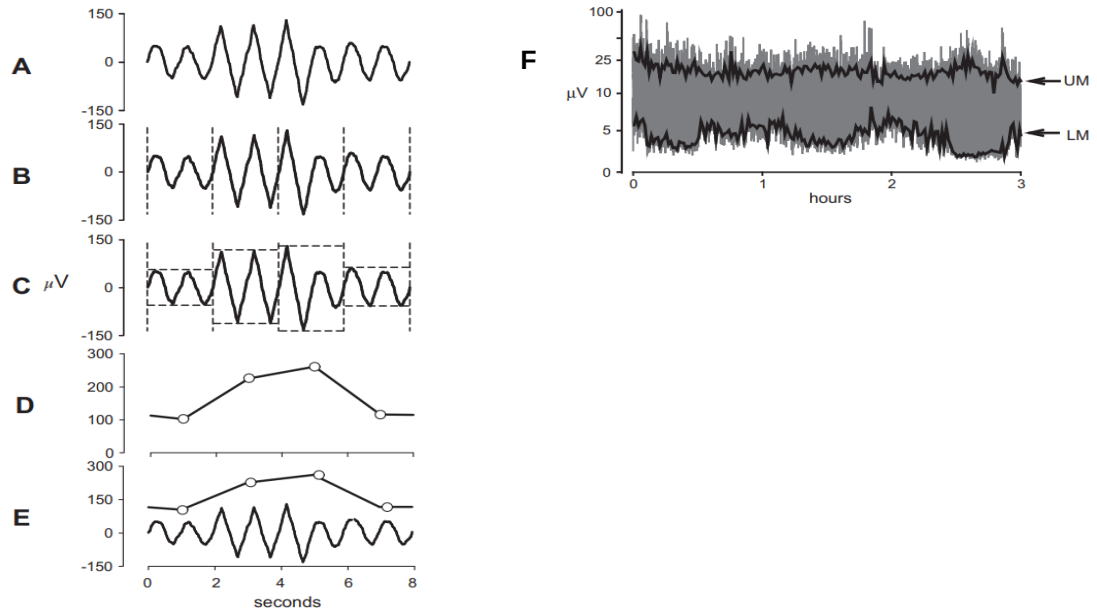

Figure 6: Scheme of the rEEG calculation based on O'Reilly et a (O'Reilly et al., 2012) with **(A)** Exemplary raw EEG signal. **(B)** Partitioning of EEG signal into adjacent intervals (dashed vertical lines). **(C)** Measurement of EEG amplitude on each adjacent interval. Numerically these values are the difference between maximal and minimal value of an interval (dashed horizontal lines). **(D)** Construction of the continuous representation of EEG amplitude. **(E)** Final continuous amplitude signals superimposed on initial EEG signal of 8 seconds. **(F)** Time compressed rEEG signal of 3 hours. Values of LM and UM are calculated as 5th and 95th percentiles of rEEG values (black arrows).

2.4.2. The Narcotrend index

The NCT Monitor, originally based on visual assessment of the raw EEG in relation to sleep classification, should help to assess state of anesthesia by offering a dimensionless, linear NCT index from 100 (awake) to 0 (electrical silence or coma) (Kreuer & Wilhelm, 2006). The NCT Monitor performs an automatic real time interpretation of 20 seconds raw EEG epochs every 5 seconds. Basis of the interpretation algorithm is the visual classification of 1000 raw EEG traces of 20 seconds. Simplified, the interpretation algorithm of the NCT Monitor can be reduced to the following steps: after artifact removal (e.g. electromyographic activity or eye movement), qEEG features are calculated from the time (e.g. autoregressive parameters) and the frequency (e.g. spectral parameters) domain. After application of multivariate classification functions and plausibility checks, the monitor reveals the linear index (Schultz A, 2004).

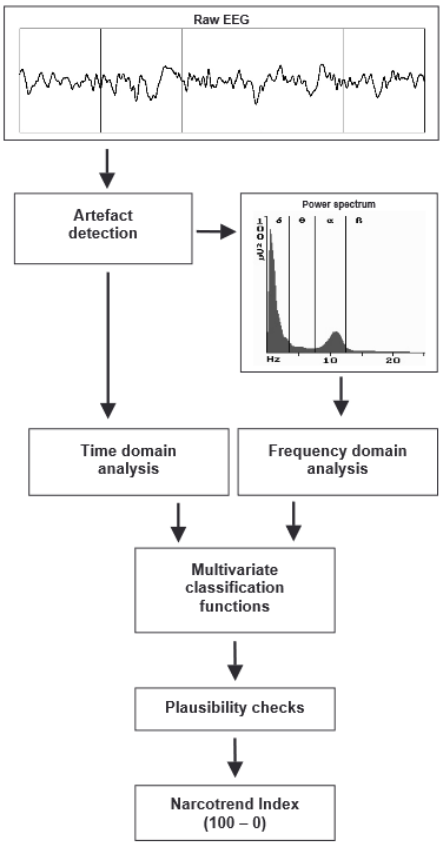

Figure 7: Scheme of the Narcotrend classification algorithm (Schultz A, 2004).

2.4.3. Electroencephalography band power

Through application of the Fast Fourier Transformation, the EEG can be decomposed into its frequency components. To provide information on the frequency components and corresponding amplitudes, the so called ´spectrogram´ illustrates the power (on the y-axis) by frequency (on the x-axis). The power corresponds to the squared amplitude value [µV] and is commonly represented in decibels [dB], defined as 10 times the log base 10 of the EEG power in the respective frequency (Purdon, Sampson, et al., 2015). To calculate the relative power of a frequency, the absolute band power of the respective frequency is divided by the absolute band power of all frequencies or a defined frequency range (I. J. Rampil, 1998). Spectral analyses aim to detect subtle changes in frequency structure due to anesthetic drug dose or effect (E. R. John, 2005; Purdon, Sampson, et al., 2015). Nevertheless, various influences can cause changes in the frequency structure of the EEG, which still need to be defined. Early attempts to measure electrical brain activity and thus the degree of consciousness used components from the power spectrum of the EEG (Gaskell et al., 2017; E. R. John, 2005). Reactions of parameters from the power spectrum to changes in cerebral saturation and to changes in the degree of consciousness are described. In the late 1990ies an increase in the

delta power is described to detect cerebral ischemia (I. J. Rampil, 1998). Current research indicates that trends in the power spectrum are related to the level of consciousness and that spectral components can serve as markers for the presence of consciousness (Choi, Noh, & Shin, 2020; Colombo et al., 2019). Literature suggests, that during general anesthesia, the highest power values are found for the slow-delta (~1 Hz) and alpha (~ 10 Hz) oscillation (Gaskell et al., 2017; John, 2005; Purdon, Sampson, et al., 2015).

2.4.4. Entropies

The entropy is related to the amount of ´disorder´ in a system and, in terms of an information theoretical context, aims to assess the irregularity, complexity, or unpredictability of a signal. Claude Shannon introduced the concept of entropy to quantify the information content within a signal and he defined it as:

$$H = - \Sigma\, p(i) \log p(i) \qquad (3)$$

Entropy, according to Shannon C.E., to quantify probabilities of an amount (i) of contributing contents (p) of the signal (Shannon, 1948).

In short, the entropy reflects the shape of a probability distribution of states. The more uniformly distributed, the higher the entropy. In the context of anesthesia research, different entropies have been introduced. We used the permutation entropy, where the information of states is derived directly from the EEG time series (Jordan, 2008) and the spectral entropy, where the information of states is derived from the power spectrum (H. Viertiö-Oja, 2004). Studies suggest that entropy parameters of the EEG are a useful tool to assess anesthetic drug effect by estimating the information content of the EEG (Bruhn, 2001). A recent study on age-related changes in the EEG indicates that entropic parameters are superior to power spectral density parameters in detecting subtle changes in the oscillatory composition of the EEG (Matthias Kreuzer et al., 2020).

2.4.4.1. Permutation Entropy

Permutation entropy, introduced by Bandt and Pompe in 2002, corresponds to the Shannon Entropy, applied to the regularity of distribution of coded amplitude values in the EEG time series (Bandt & Pompe, 2002). Permutation entropy is computed on the time-domain of the EEG and quantifies the regularity structure of the neighboring order

of amplitude values in time series. Hence, permutation entropy provides information about the uniformity of the distribution of ordinal EEG patterns (Matthias Kreuzer et al., 2020). The more uniformly distributed the patterns of the ranks of neighboring of amplitude values is, the higher the permutation entropy. Studies indicate that permutation entropy is able to separate wakefulness from unconsciousness and can serve as a surrogate of local cortical information processing (Ranft et al., 2016). It is considered as a surrogate of cortical information processing

$$H = - \Sigma\, p(\pi) \log p(\pi) \qquad (4)$$

Permutation entropy to reflect the uniformity of distribution of neighboring order of amplitude values on the time domain of the EEG (Bandt & Pompe, 2002).

2.4.4.2. Spectral Entropy

The spectral entropy is derived from the power spectrum of the EEG. Based on the Shannon entropy, the spectral entropy evaluates the shape of the relative power spectrum, i.e., it defines the percentual contribution of the power of each frequency to the total power in a defined frequency range. The more uniformly distributed the relative power spectrum is, the higher the spectral entropy. As the EEG under general anesthesia, induced and maintained with common anesthetics, changes from a high frequency, low amplitude pattern to one with slow oscillations and high amplitudes, the spectrum also changes from a more uniform distribution (high spectral entropy) to a more left skewed distribution (low spectral entropy).

$$S = - \Sigma\, p(f_i) \log p(f_i) \qquad (5)$$

Spectral entropy to reflect the uniformity of contribution of the power of each frequency to the total power of the EEG (H. Viertiö-Oja, 2004).

2.5. Statistical analyses

To describe a possible relationship between the NIRS and the (processed) EEG parameter we constructed linear models that describe the relationships between these factors under controlled conditions, i.e., within the defined temperature, MAP, and aaMAC ranges as well as only for the intraoperative period until clamping.

Therefore, we used the MATLAB *fitlm* function and included only one factor (y ~ 1 + x1). This factor is represented by different EEG parameters, trying to regard the whole spectrum from the older, more basic, to the more current approaches of EEG analyses. The MATLAB fitlm properties include information about following coefficient estimates for the slope of the graph and the intercept (with the y-axis): estimated coefficient value (*Estimate*), Standard error of the estimate (*SE*), t-statistic (*tStat*) and p-value (*pValue*). The t-statistic tests the null hypothesis, that the slope is zero against the alternative that it is different from zero, and the p-value is calculated for this t-statistic on 5% significance level. A $p < 0.05$ indicates a significant different slope from zero. Hence it indicates a significant increase or decrease of the EEG parameter with NIRS at the 5% significance level.

The MATLAB fitlm properties also include information about following summary statistics: the *number of observations* and the *R-squared* value. The R-squared value is the portion of the total sum of squares explained by the model, and thus suggests the portion of variability of the EEG parameter that can be explained by the model. A R-squared of e.g. 0.02 would suggest that 2% of the EEG variability can be explained by the model.

More information on the MATLAB fitlm function, illustrated with examples, can be found on “https://de.mathworks.com/help/stats/linearmodel.html”.

As the duration of the analyzed period shows a high dispersion within the cohort, mainly between 20 and 150 minutes (figure 9), and as EEG variables are not normally distributed, the median was calculated individually for each patient instead of presenting pooled data as done for the 3D-histograms. This method should avoid overestimating individual patients. NIRS values from 30% to 100% were considered in steps of 1%. Consequently, it cannot be read out of the figures how long or often each patient reveals this certain NIRS value during the analyzed period, but it prevents overemphasis of patients with long interventions.

For the case reports, we compared the patients with ´mild´ desaturation (n = 5) and with ´severe´ desaturation (n = 4) using a Mann–Whitney U test at a confidence level of 95%

together with the area under the receiver operator characteristics curve and 10,000-fold bootstrapped 95% CIs as effect size. We used the MATLAB-based MES toolbox for area under the receiver operator characteristics curve and 95% CI calculation (Hentschke & Stüttgen, 2011). According to the traditional academic point system, area under the receiver operator characteristics curve values can be interpreted as ´excellent´ (area under the receiver operator characteristics curve between 1 and 0.9); ´good´ (area under the receiver operator characteristics curve less than 0.9, but greater than or equal to 0.8); ´fair´ (area under the receiver operator characteristics curve less than 0.8, but greater than or equal to 0.7); ´poor´ (area under the receiver operator characteristics curve less than 0.7, but greater than or equal to 0.6); or ´fail´ (area under the receiver opera-tor characteristics curve less than 0.6). For the (normalized) power spectral density comparison, we only defined significant results if at least two neighboring frequencies showed significant differences between the group with ´mild´ and ´severe´ desaturation. This or similar approaches were used earlier (Akeju et al., 2014; Matthias Kreuzer et al., 2020). All tests applied were two-tailed tests and we considered $p < 0.05$ to be significant.

2.5.1. Range Electroencephalography and Near Infrared Spectroscopy

The linear regression model aims to investigate the relationship between rEEG and NIRS value. The rEEG signal was first decomposed into alpha (8 - 12 Hz), beta (12 - 25Hz), delta (0.5 - 4 Hz) and theta (4 - 8 Hz) frequency bands. Whenever one individual patient showed a certain saturation during the whole analyzed time period, the corresponding rEEG parameter (UM, LM and BW [µV]) was stored in each frequency band. In separated linear models, the median of either upper margin, lower margin or bandwidth is represented as a function of the corresponding NIRS value. One cross represents the median rEEG of one patient, simultaneously observed with a certain NIRS value throughout the whole analyzed period but independently from the duration of this certain NIRS value. The regarded NIRS values range from 30 - 100% in steps of +1%. NIRS values below 30% were not included to avoid falsely low measurements.

2.5.2. Narcotrend index and Near Infrared Spectroscopy

The behavior of a pEEG parameter, represented by the NCT index, in relation to the current cerebral saturation, evaluated with NIRS, was investigated as well. Since the analyzed EEG tracks were recorded with the NCT monitor, a linear model of the NCT index and the NIRS value was also calculated for the sake of completeness. It is

emphasized that this retrospective research did not venture an assessment of the monitor. However, this analysis could provide useful impulses for future studies on the behavior of the NCT index in relation to current cerebral saturation, in order to make the monitor more applicable. It might even help to clarify whether pEEG monitors are capable to detect brain ischemia.

2.5.3. Spectral Encephalography and Near Infrared Spectroscopy

Putting the behavior of absolute or relative power in linear relation to the course of cerebral saturation can help to identify saturation induced changes of the EEG spectral power. Our analyses of absolute and relative band power of the alpha (8 - 12 Hz), beta (12 - 25 Hz), delta (0.5 - 4 Hz) and theta (4 - 8 Hz) frequency aim to investigate their relationship to cerebral saturation. In separated linear models, the median of either absolute or relative power of each frequency band is represented as a function of the corresponding NIRS value. One cross represents the median power of the EEG of one patient, simultaneously observed with a certain NIRS value throughout the whole analyzed period but independently from the duration of this certain NIRS value. The regarded NIRS values range from 30 - 100% in steps of +1%.

2.5.4. Entropy and Near Infrared Spectroscopy

We also regarded entropic parameters in order to investigate saturation-related changes in the EEG from the 0.5 - 30 Hz range. We analyzed permutation entropy (PEn), which is calculated directly from the raw EEG, and spectral entropy (SpEn), which is calculated from the frequency spectrum of the EEG. More information about the entropy term and the mathematical background can be found in corresponding literature (H. Viertiö-Oja, 2004).

2.5.4.1. Permutation Entropy and Near Infrared Spectroscopy

This linear regression model on PEn and NIRS aims to investigate whether this entropic parameter can be influenced by the cerebral saturation. One cross represents the median PEn of the EEG of one patient, simultaneously observed with a certain NIRS value throughout the whole analyzed period but independently from the duration of this certain NIRS value. The regarded NIRS values range from 30 - 100% in steps of +1%.

2.5.4.2. Spectral Entropy and Near Infrared Spectroscopy

The SpEn corresponds to the Shannon Entropy, applied to the power spectrum of the EEG. This method is computed on the frequency-domain of the EEG and aims to assess brain activity by measuring the regularity of frequency distribution from the power spectrum of the EEG (J. Bruhn et al., 2006) and finds implementation in the commercially available entropy modules. This linear regression model on SpEn and NIRS aims to investigate whether this entropic parameter can be influenced by the cerebral saturation. One cross represents the median SpEn of the EEG of one patient, simultaneously observed with a certain NIRS value throughout the whole analyzed period but independently from the duration of this certain NIRS value. The regarded NIRS values range from 30 - 100% in steps of +1%.

2.6. Exemplary investigations of patients with ´mild´ or ´severe´ cerebral desaturation

We analyzed frontal NIRS and EEG recordings during cardiac surgery under Isoflurane. We visually selected 9 patients from the cohort of 307 with a constant decline of cerebral saturation, evaluated with NIRS, at stable gas concentration and without the occurrence of EEG burst suppression. For this selection we regarded the entire eligible recordings from the operation room and not only the recordings before initiation of CPB. We calculated the spectral entropy from a 10 second EEG period including for the 0.24 to 31.98 Hz range at high (%-NIRS before desaturation) and low (%-NIRS after desaturation) saturation within each patient. We defined the desaturation as ´mild´ (desaturation not below 50%-NIRS) and ´severe´ (desaturation below 50%-NIRS) and noted whether the spectral entropy has increased or decreased during the cerebral desaturation for each patient. We further compared the spectral EEG features, i.e. the power spectral density (PSD) from a 10 second EEG epoch, between the patients after ´mild´ and after ´severe´ desaturation. To compare the PSD of both cerebral desaturation groups, we calculated the AUC with 95% confidence intervals.

3. Results

3.1. Demographics

Following figures illustrate the patients` demographic variables providing median (□) and mean (+) of the male (green) and female (orange) patients. Each spot represents one patient.

Median (with IQR) and mean (with SD) age in the male population was 67 (13) and 64.75 (11.68), similar to 67 (16) and 64.34 (14.31) within the female. Median (with IQR) and mean (with SD) BMI [kg/m²] in the male population was 27.14 (6.22) and 27.81 (4.66) compared to 25.84 (9.35) and 27.20 (5.82) in the female. The cohort consisted of 221 (72%) male and 86 (28%) female patients (figure 8).

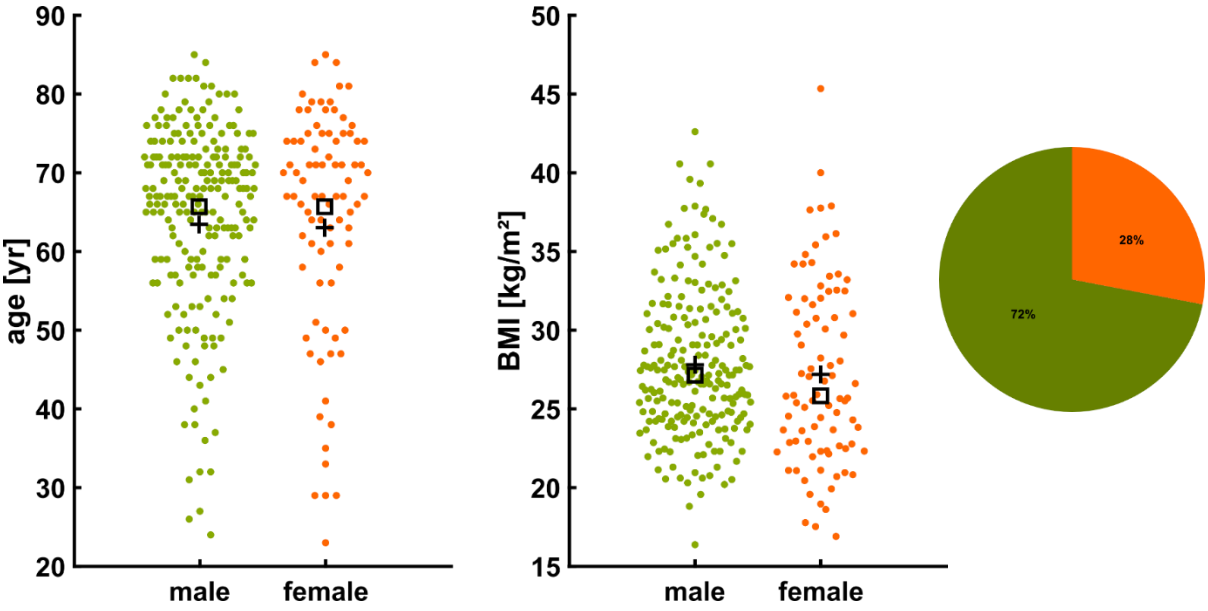

Figure 8: Demographics of 307 cardiac patients for the analyses.

Only the period from start of recording in the operating room until aortic clamping before initiation of CPB was investigated, in order to minimize interventional artefacts or uncertainties due to the retrospective approach. For example, at the beginning of the CPB the blood circulation is commonly diluted with 1400 - 1600 ml Ringer's solution, which leads to a significant drop in cerebral saturation. Not only at initiation but for the whole period on CPB the measured NIRS values may differ from those before connection to the CPB (Bennett, Weatherall, Webb, Dudnikov, & Lloyd, 2015). Further,

the oxygen demand of some patients can be reduced by cooling down the body temperature and barbiturate administration, so that unphysiological NIRS values are no longer representative for the cohort (C. B. Lewis & Adams, 2020). The duration of the investigated period varies within the cohort, ranging from a minimum of 19.8 minutes to a maximum of 6 hours and 42 minutes. Median (with IQR) and mean (with SD) time until aortic clamping is 69.03 (53.8) and 75.70 (45.56) minutes (figure 9).

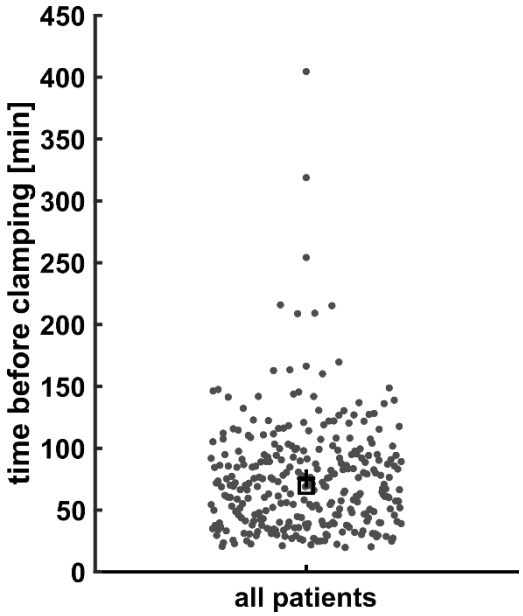

Figure 9: Duration of analyzed period per patient in minutes.

3.2. Distribution of Near Infrared Spectroscopy values

To provide information on the behavior of the NIRS signal during the investigated period, the minima, maxima and mean measured NIRS values as well as interhemispheric differences were evaluated for each patient. The two separated clouds of data points do not differentiate between sex anymore, but between left and right hemisphere. For each NIRS value, median (□) and mean (+) are presented. Median (with IQR) and mean (with SD) observed maximal NIRS value were 77% (9%) and 77.2% (7.3%) for the left hemisphere and 78% (8%) and 77.5% (7.6%) for the right. Median and mean observed minimal NIRS value was 64.5% (13%) and 62.4% (11.8%) for the left hemisphere and 64% (13%) and 62.6% (11.5%) for the right. The median and mean difference between maximum and minimum of observed NIRS value was 12% (10%) and 14.8% (10.8%) for the left and 13% (11%) and 14.9% (10.2%) for the right hemisphere (figure 10).

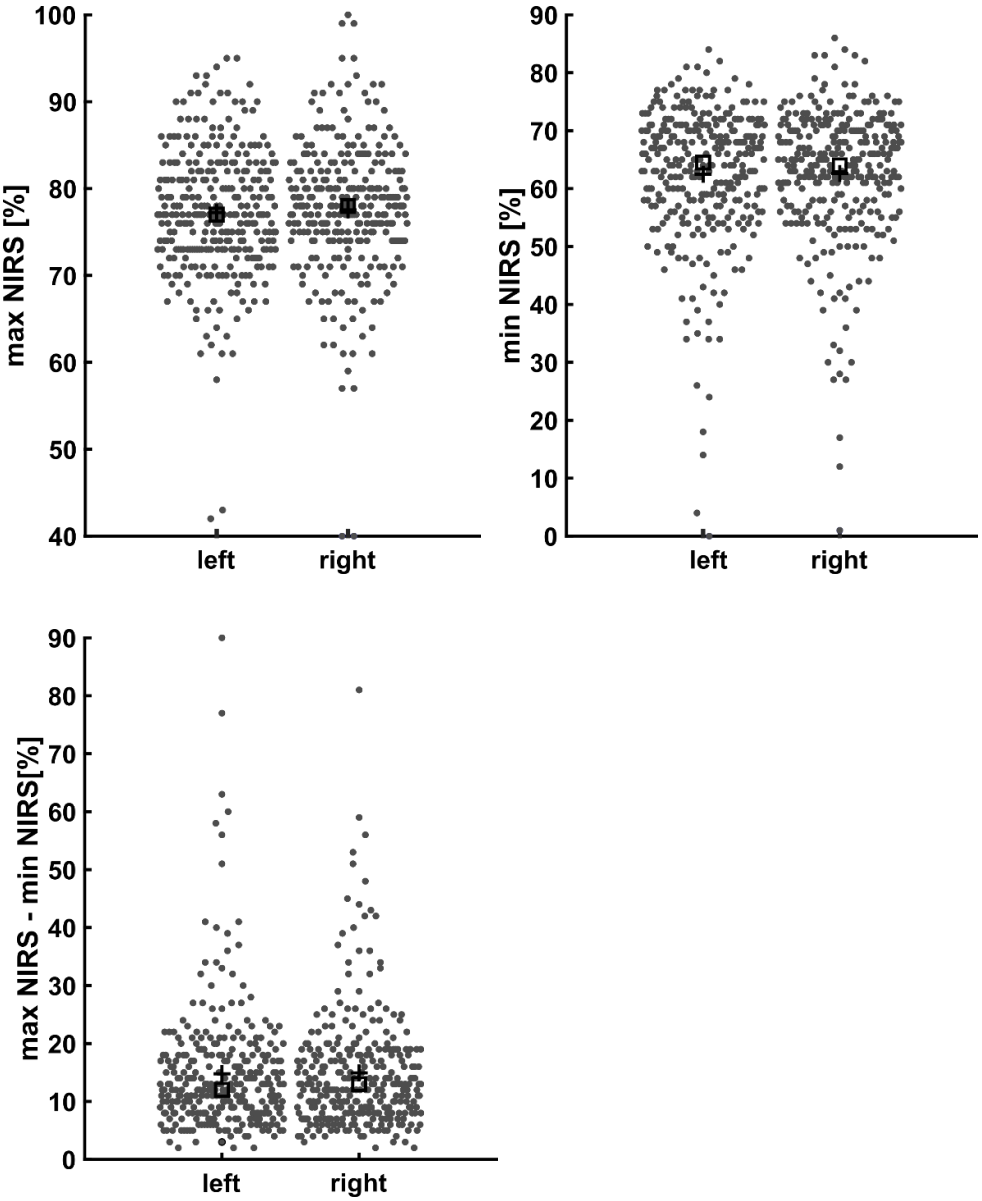

Figure 10: Maximum, Minimum and the range of NIRS values per patient.

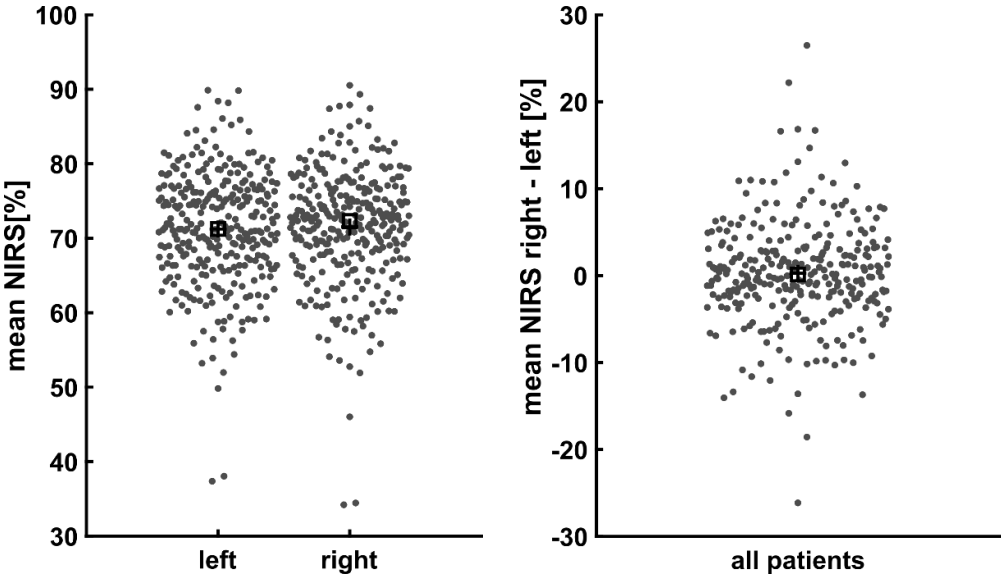

Figure 11: Mean NIRS value and interhemispheric difference of the mean for each patient.

Figure 11 illustrates median (with IQR) and mean (with SD) individual mean NIRS value with 71.3% (10.1%) and 71.2% (7.7%) for the left and 72.3% (8.7%) and 71.5% (7.7%) for the right hemisphere. Finally, the difference between mean NIRS value observed over the left and right hemisphere was calculated to show whether the values are distributed symmetrically: the median (with IQR) and mean (with SD) difference was -0.1% (5.7%) and -0.3% (6%). A calculated difference approximately being zero indicates a symmetrical displayed NIRS value for the left and right hemisphere (figure 11).

3.3. Distribution of the range Electroencephalography parameters of the pooled data: 3D-histograms

Figure 12 shows the 3D-histograms of the rEEG-NIRS-aaMAC for the triplets pooled from all patients. For clarity, triplets are only presented if they occurred at least 25 times in the data set. The added color bar codes for the number of observations on a logarithmic scale. Twelve diagrams are presented for the three main components of the rEEG (UM, LM and BW) within the alpha (8 - 12 Hz), beta 12 - 25 Hz), delta (0.5 - 4Hz) and theta (4 - 8 Hz) frequency. Because different patients contribute differently to these plots, we present the histograms only to give an impression of the data and performed statistics on data that was averaged for each patient.

The resulting 3D-histograms of the distribution of NIRS, rEEG and aaMAC values in pooled manner illustrate the heterogenetic distribution of the biosignals and again, the necessity to control for the aaMAC to be within the targeted range of 0.6 - 0.8 for further analyses. Each 3D-histogram can be found individually per frequency and per rEEG parameter in the appendix on a larger scale.

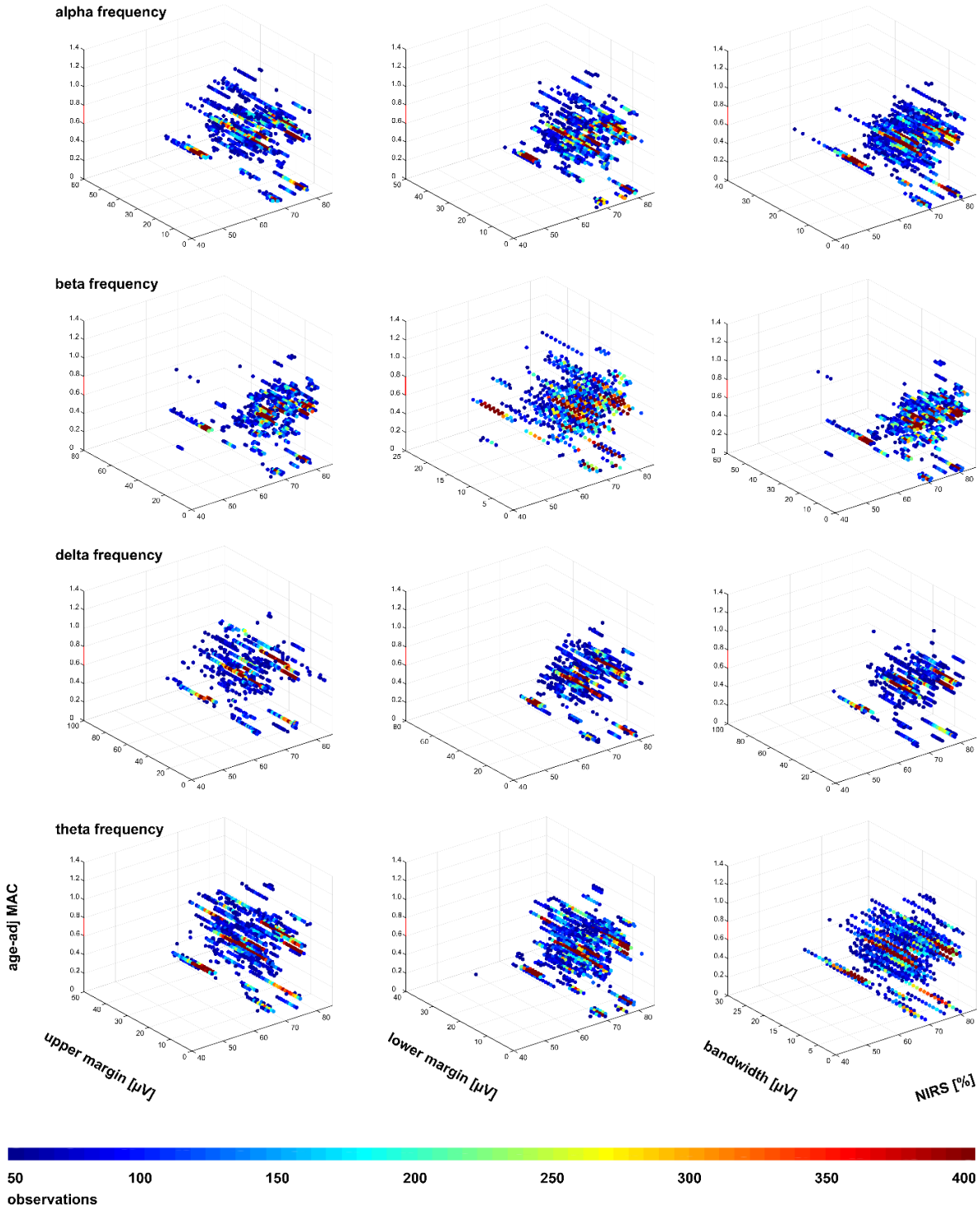

Figure 12: Overview of the diagrams of rEEG, NIRS and aaMAC values.

3.4. Linear Regression models between Electroencephalography parameters and Near Infrared Spectroscopy

We used the linear regression models for initial investigations regarding a possible relationship between the NIRS and the EEG: Therefore, we included the median EEG parameter for each NIRS value from each patient (that was recorded within the temperature, MAP, and MAC limits). This approach can correct for different intervention durations, so that no patient becomes over-emphasized in the data set. But of course, not each patient showed each NIRS value, so the number of patients included in the analysis for each NIRS value was different.

3.4.1. Range Electroencephalography and Near Infrared Spectroscopy

To present the results of the linear model on rEEG and NIRS, we provide three diagrams (regarding UM, LM and BW) per frequency range, i.e., for the alpha-, beta-, delta-, and theta-band.

The linear regression model on the relation between alpha frequency rEEG and NIRS indicates a statistically significant increase of the UM ($p = 0.009$) and LM ($p < 0.001$) value (slope +0.11 and +0.09) with increasing NIRS signal. Consequently, the BW did not show a significant change with NIRS. Table 6 presents the statistical parameters in detail.

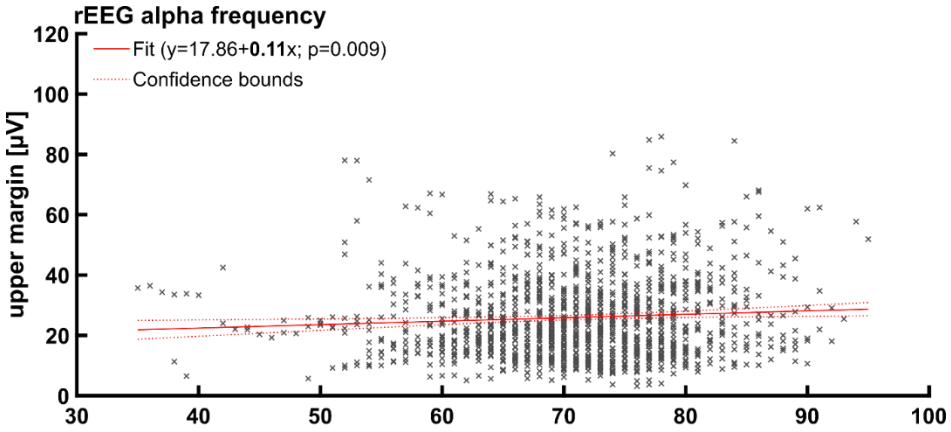

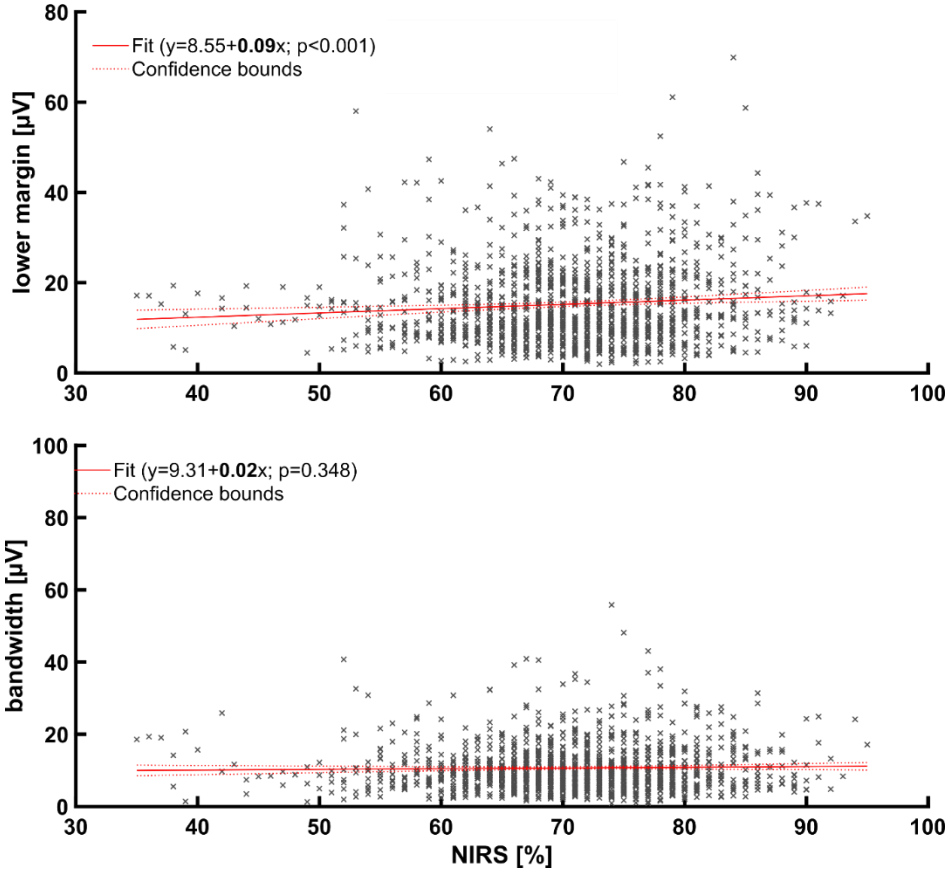

Figure 13: Linear model on the alpha frequency rEEG and NIRS with linear equation.

alpha frequency	Estimate	SE	p-value (t-stat)	R-squared	number of observations
UM slope	0.11	0.04	0.009 (2.64)	0.005	1334
intercept	17.86	3.08			
LM slope	0.09	0.03	<0.001 (3.32)	0.008	1334
intercept	8.55	2.03			
BW slope	0.02	0.02	0.348 (0.94)	0.0007	1334
intercept	9.31	1.46			

Table 6: Properties of the linear model on the alpha frequency rEEG and NIRS.

Similar to the findings in the alpha frequency, the linear regression model on the relation between beta frequency rEEG and NIRS indicates a statistically significant increase of the UM ($p = 0.007$) and LM ($p < 0.001$) value (slope: +0.10 and +0.07) with increasing NIRS signal. Consequently, the BW did not show a significant change with NIRS. Table 7 presents the statistical parameters in detail.

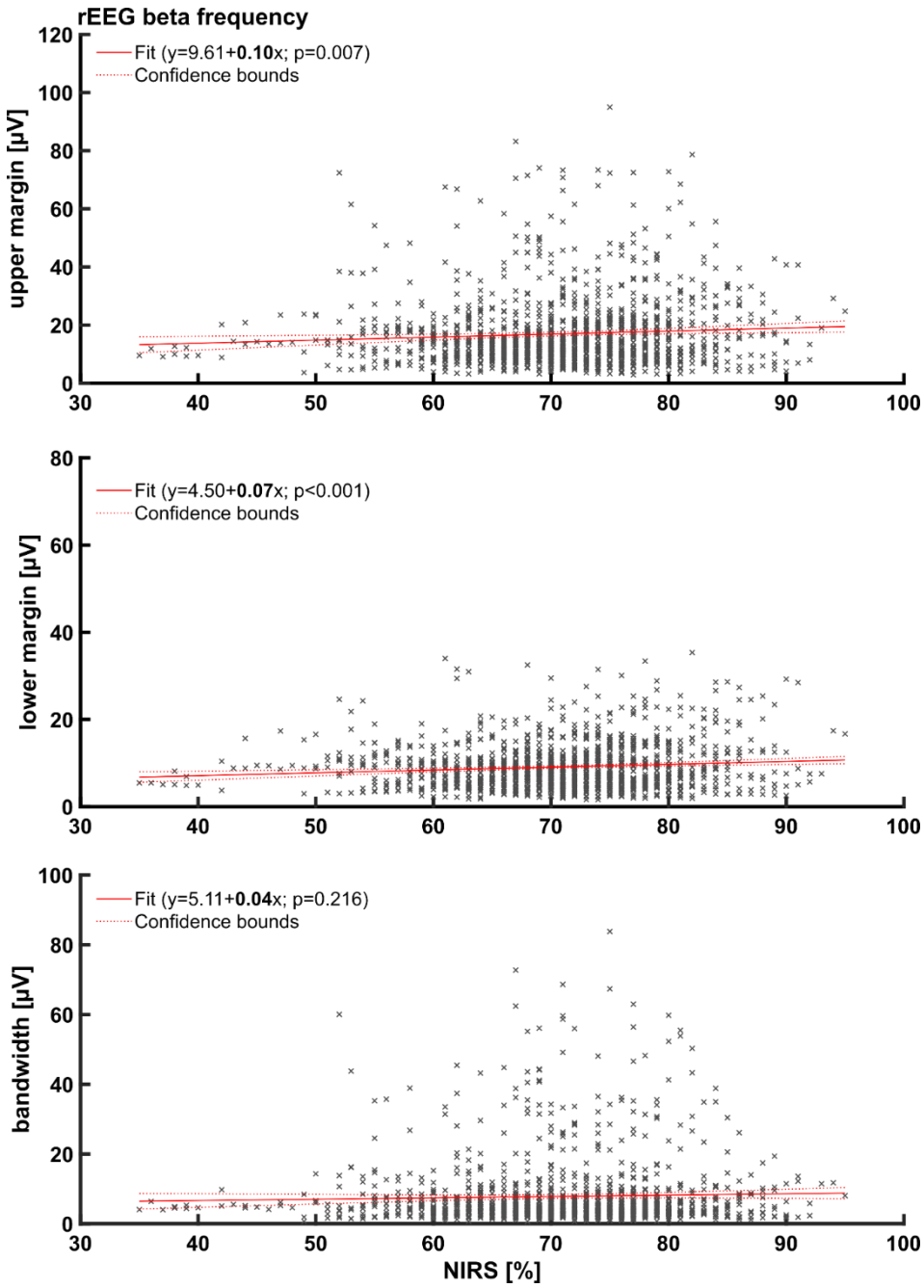

Figure 14: Linear model on the beta rEEG and NIRS with linear equation.

beta frequency	Estimate	SE	p-value (t-stat)	R-squared	number of observations
UM slope	0.10	0.04	0.007 (2.72)	0.006	1334
intercept	9.61	2.73			
LM slope	0.07	0.02	<0.001 (3.95)	0.011	1334
intercept	4.50	1.18			
BW slope	0.04	0.03	0.216 (1.24)	0.001	1334
intercept	5.11	2.23			

Table 7: Properties of the linear model on the beta rEEG and NIRS.

The linear regression model on the relation between delta frequency rEEG and NIRS indicates a statistically significant decrease of the UM ($p = 0.018$) and BW ($p < 0.001$) value (slope: -0.13 and -0.14) with increasing NIRS signal. The change in the LM was not statistically significant. In contrast to the increasing alpha and beta rEEG parameters, the delta rEEG parameters decreased with increasing NIRS. This suggests that the higher frequencies of the EEG react in the opposite way to the current cerebral saturation than the lower delta frequency. Table 8 presents the statistical parameters in detail.

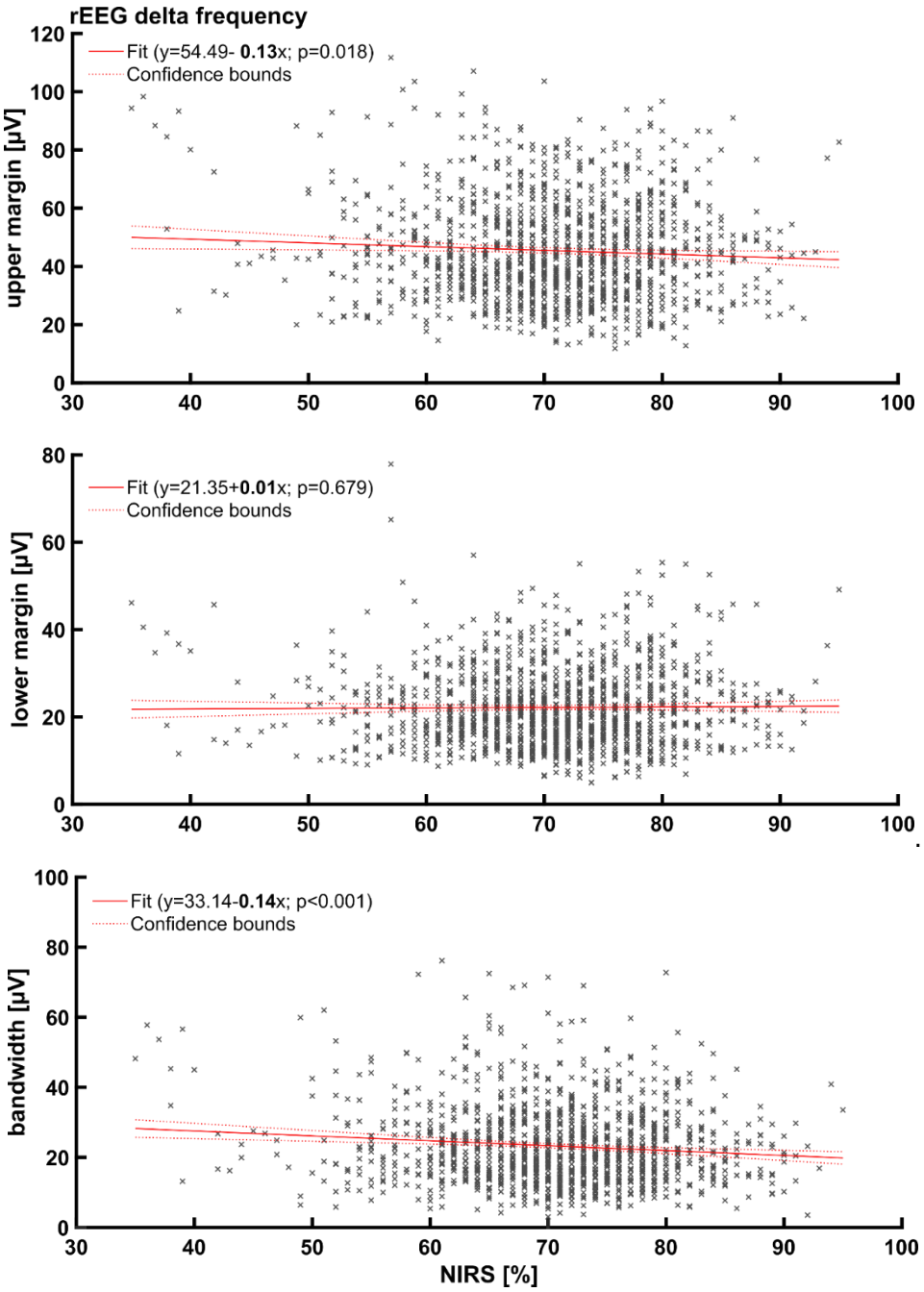

Figure 15: Linear model on the delta rEEG and NIRS with linear equation.

delta frequency	Estimate	SE	p-value (t-stat)	R-squared	number of observations
UM slope	-0.13	0.05	0.018 (-2.36)	0.004	1334
intercept	54.50	3.86			
LM slope	0.01	0.03	0.679 (0.41)	<0.001	1334
intercept	21.35	2.00			
BW slope	-0.14	0.04	<0.001 (-3.99)	0.012	1334
intercept	33.14	2.50			

Table 8: Properties of the linear model on the delta rEEG and NIRS.

The linear regression model on the relation between theta frequency rEEG and NIRS indicates a statistically significant increase (p = 0.025; slope: +0.04) of the LM and decrease (p = 0.016; slope: -0.04) of the BW value with increasing NIRS signal. The UM does not change in a statistically significant way. Table 9 presents the statistical parameters in detail.

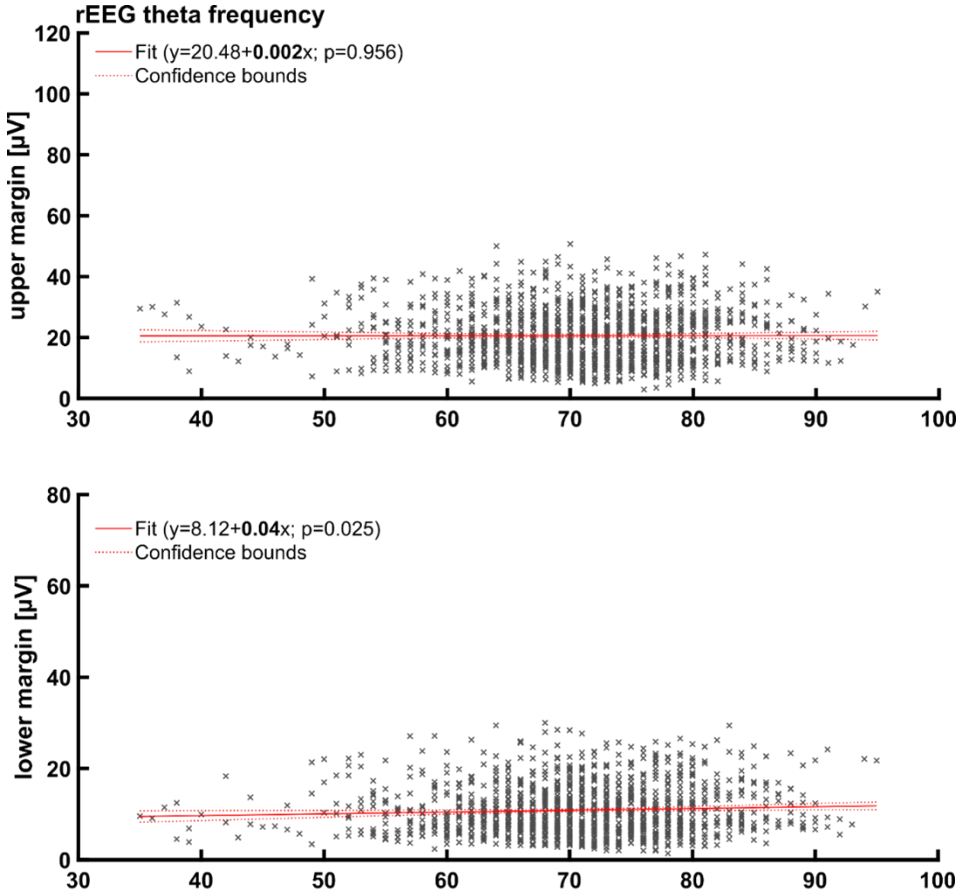

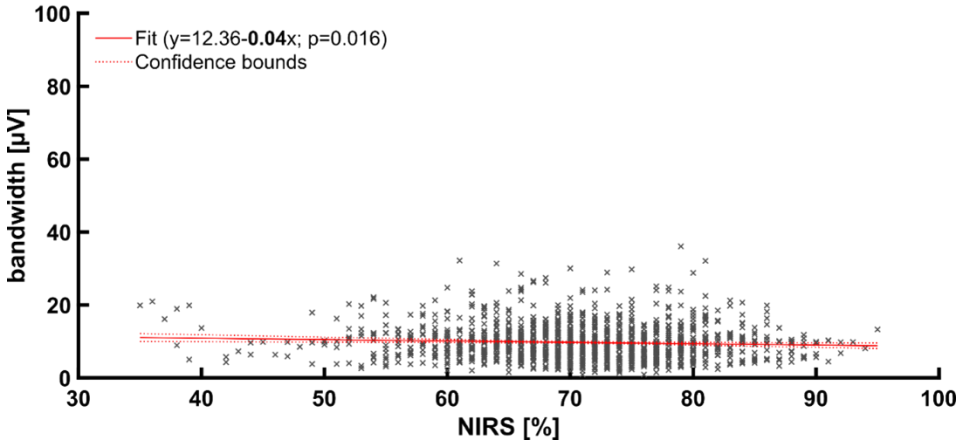

Figure 16: Linear model on the theta rEEG and NIRS with linear equation.

theta frequency	Estimate	SE	p-value (t-stat)	R-squared	number of observations
UM slope	0.002	0.03	0.956 (0.06)	<0.001	1334
intercept	20.48	1.98			
LM slope	0.04	0.02	0.025 (2.25)	0.004	1334
intercept	8.12	1.23			
BW slope	-0.04	0.02	0.016 (-2.42)	0.004	1334
intercept	12.36	1.10			

Table 9: Properties of the linear model on the theta rEEG and NIRS.

In summary, the rEEG analyses show, that the relation of EEG changes and NIRS signal differ between the four frequency bands and also between the the three main parameters of the rEEG within each frequency band. Therefore it is useful to pick out specific EEG parameters for future investigation of any saturation related changes in the EEG. Regarding our analyses, a statistically significant increase with increasing NIRS value was found for following rEEG parameters: UM and LM of the alpha and beta frequency- and LM of the theta frequency-rEEG. On the other hand, we found a statistically significant decrease with increasing NIRS value for following rEEG parameters: UM and BW of the delta frequency- and BW of the theta frequency-rEEG. The shift towards lower (r)EEG amplitudes in the higher frequencies and towards higher (r)EEG amplitudes in the lower frequencies presents changes towards an EEG indicative of a deeper level of anesthesia. However, in this case the EEG change may actually be caused by a change in saturation.

To supplement and simplify the finding, figure 17 shows the changes in rEEG in a schematic fashion:

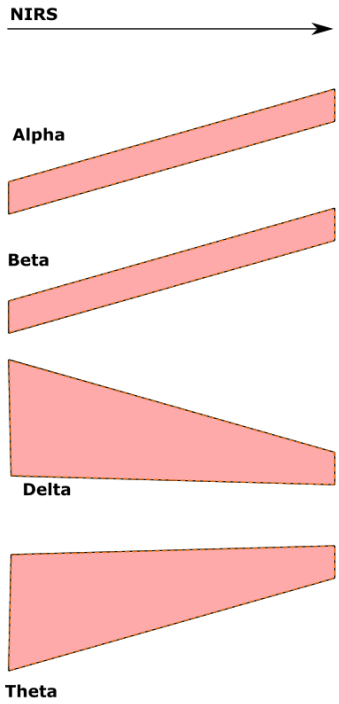

Figure 17: Scheme of the rEEG changes in the different frequencies with increasing NIRS.

3.4.2. Narcotrend and Near Infrared Spectroscopy

The linear regression between the NIRS and NCT indices may reflect the current clinical situation as the NCT is used to monitor the patient's perioperative hypnotic level. The linear regression model on the relation between NCT index and NIRS indicates a statistically significant increase: NCT index = 0.08 x NIRS + 37.69 ($p = 0.049$; t-stat = 1.97; R-squared = 0.002). We observed a few NCT Indices = 99, indicative of either an awake patient, or, if the anesthesiologist can confirm the unconsciousness of the patient, indicative of undetected burst suppression. Monitoring systems were reported to confuse the EEG of the awake state with the EEG of burst suppression (S. M. Hart, 2009). To avoid this pitfall, we excluded NCT Indices of 99, and then found a regression of NCT index = 1.14 x NIRS + 33.34 as displayed in figure 18 and table 10.

By visual assessment of the linear model, one sees that the NCT indices, which correspond to lower cerebral saturation (NIRS < 40%) were exclusively below 40 after removing the NCT Indices = 99. Hence, the NCT index seems to be susceptible to changes in oxygen saturation as reflected by NIRS at controlled conditions.

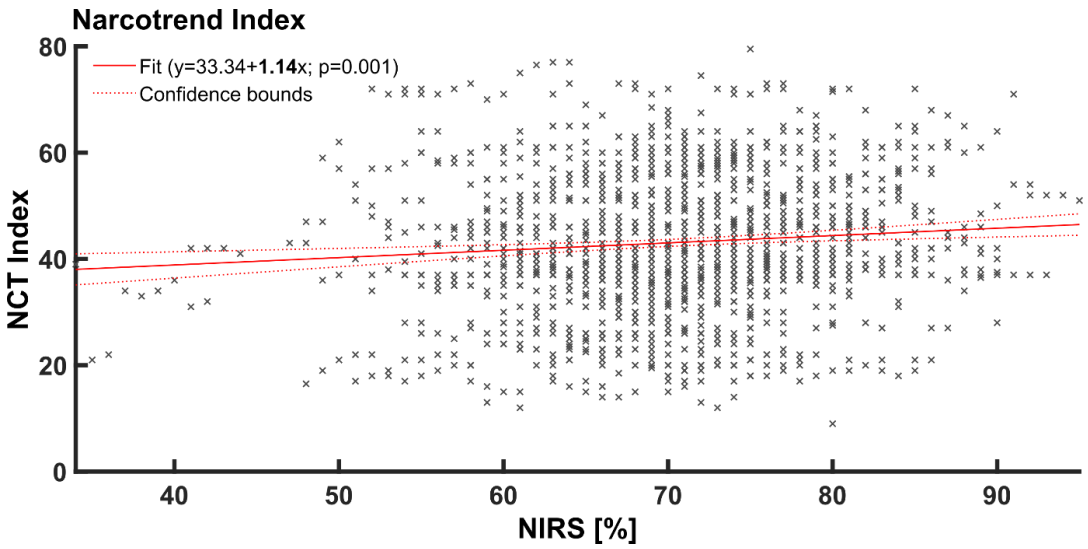

Figure 18: Linear model on the NCT index and NIRS with linear equation.

NCT index	Estimate	SE	p-value (t-stat)	R-squared	number of observations
slope	1.14	0.04	0.001 (3.48)	0.007	1659
intercept	33.34	2.83			

Table 10: Properties of the linear model on the NCT index and NIRS.

3.4.3. Spectral analyses and Near Infrared Spectroscopy

Decomposing the EEG in the four frequency bands, i.e., the alpha, beta, delta and theta band, allows the comparison of the frequency components and its amplitudes. In our linear model, only the relative power in the alpha frequency band showed a statistically significant relationship to the NIRS value. Both, absolute and relative power values increased with increasing NIRS, however only the relative power increased (slope +0.042) in statistically significant way. Figure 19 presents the corresponding plots for only the alpha frequency range while table 11 contains all statistical details for all four frequency bands.

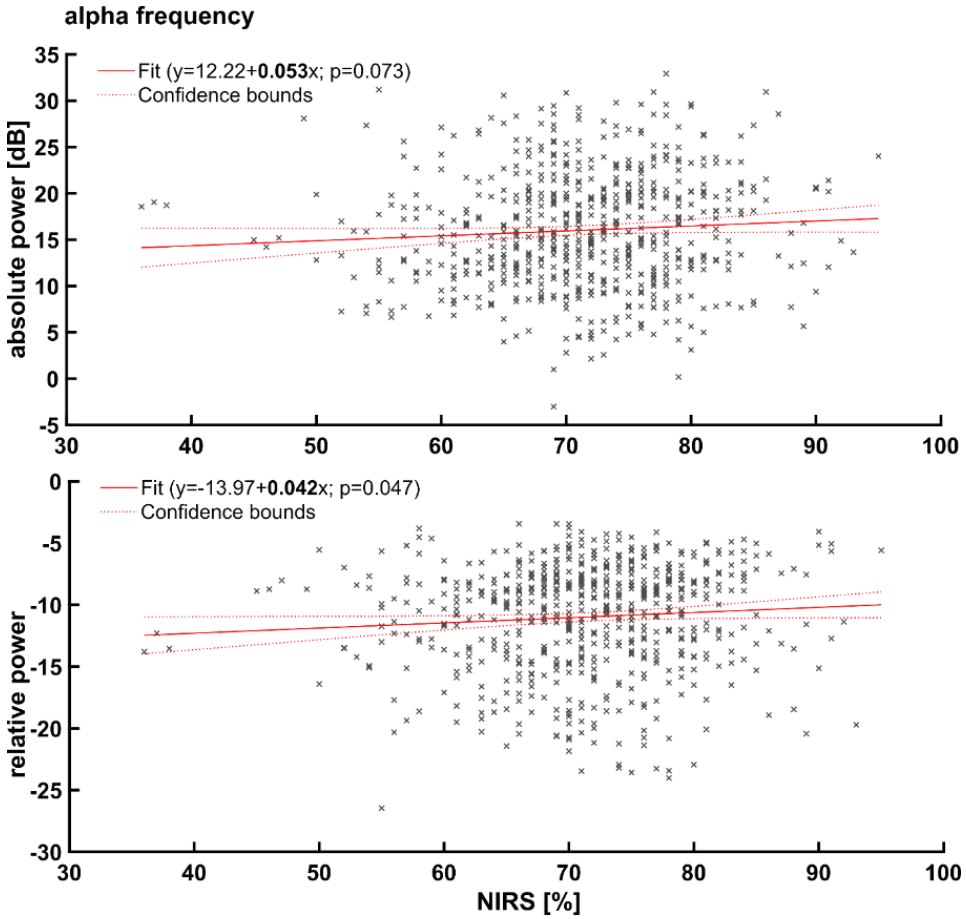

Figure 19: Linear model on the absolute and relative power in the alpha frequency range 8 - 12 Hz and NIRS with linear equation.

	Estimate	SE	p-value (t-stat)	R-squared	number of observations
alpha frequency					
absolute power					
slope	0.05	0.03	0.073 (1.80)	0.005	638
intercept	12.22	2.13			
relative power					
slope	0.04	0.02	**0.047 (1.99)**	0.006	638
intercept	-13.97	1.51			
beta frequency					
absolute power					
slope	0.03	0.03	0.456 (0.75)	0.001	638
intercept	8.81	2.45			
relative power					
slope	0.01	0.02	0.543 (0.61)	0.001	638
intercept	-17.38	1.67			
delta frequency					
absolute power					
slope	0.003	0.03	0.898 (0.13)	<0.001	638
intercept	25.23	1.93			
relative power					
slope	-0.01	0.01	0.168 (-1.38)	0.003	638
intercept	-0.96	0.41			
tetha frequency					
absolute power					
slope	0.02	0.03	0.441 (0.77)	0.001	638
intercept	14.76	2.13			
relative power					
slope	0.01	0.01	0.421 (0.81)	0.001	638
intercept	-11.43	1.02			

Table 11: Properties of the linear model on the alpha, beta, delta and theta band power and NIRS.

3.4.4. Entropy analyses and Near Infrared Spectroscopy

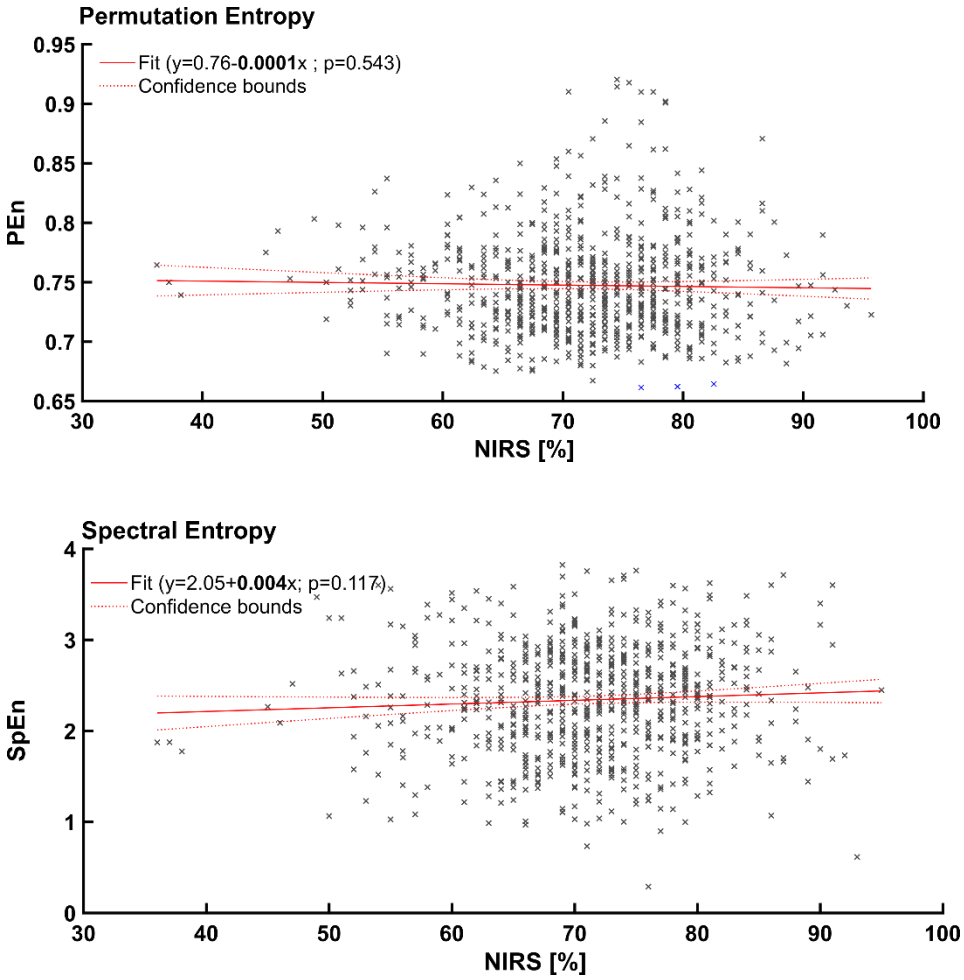

Figure 20: Linear model on the permutation entropy (PEn), spectral (SpEn) entropy and NIRS with linear equation.

	Estimate	SE	p-value (t-stat)	R-squared	number of observations
PEn					
slope	-0.0001	<0.001	0.543 (-0.621)	<0.001	788
intercept	0.76	2.13			
SpEn					
slope	0.004	0.003	0.117 (1.57)	0.003	788
intercept	2.05	0.19			

Table 12: Properties of the linear model on the permutation entropy (PEn), spectral entropy (SpEn) and NIRS.

The linear regression model on the relation between neither PEn nor SpEn and NIRS indicates a statistically significant change of the entropic EEG parameters with increasing NIRS signal. Although, not significant (p = 0.117), the increase of SpEn, which serves as a proxy for a clinically used monitor (Matthias Kreuzer et al., 2020), may still add valuable information.

3.5. Exemplary Electroencephalography analyses during events of desaturation

For all patients, except for one, with ´mild´ cerebral desaturation (NIRS not below 50%), we observed a decrease in SpEn, a parameter behavior also observed with increasing anesthetic level. In contrast, we found a SpEn increase for all patients with ´severe´ cerebral desaturation (NIRS below 50%). An increase in SpEn can also be indicative for an arousal reaction. All these results were obtained at stable gas concentrations during constantly decreasing cerebral saturation, evaluated with NIRS. Table 13 presents the measured NIRS values before and after the desaturation event with the calculated SpEn change from the related 10-second-EEG epochs. Figure 21 presents the extent of desaturation (on the left) with the calculated SpEn values from the related EEG epoch (on the right) by connected start and end values of the event.

NIRS high [%]	**NIIRS low [%]**	**SpEn change**
Desaturation below 50%		
67	37	**increase**
66	46	**increase**
61	48	**increase**
58	49	**increase**
Desaturation not below 50%		
67	52	**decrease**
68	56	**decrease**
66	57	increase
68	60	**decrease**
73	60	**decrease**

Table 13: Absolute NIRS value [%] before and after the desaturation event (left) with concomitant SpEn change (right) of 9 patients.

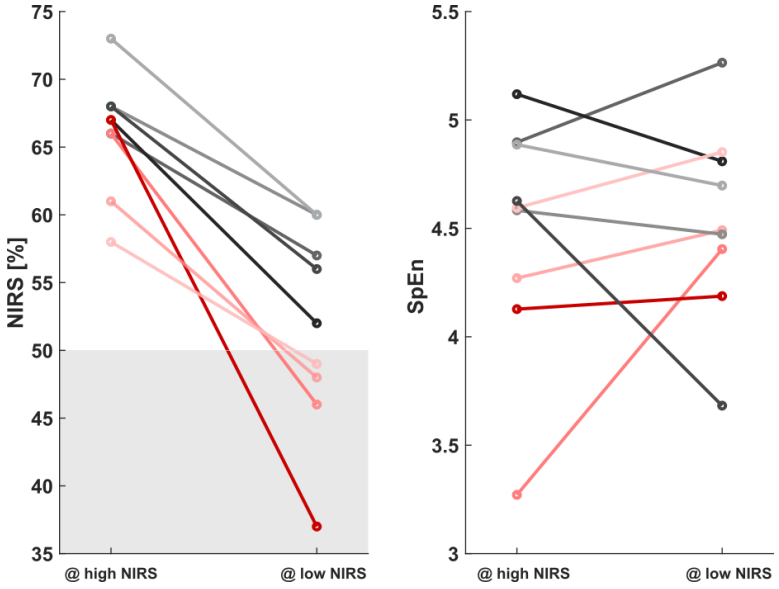

Figure 21: NIRS value before and after the desaturation event (left) with concomitant SpEn value (right) from 9 patients.

The observation of the spectral EEG features after the desaturation revealed higher delta-band power as well as lower alpha- and beta-band power in the patients with ´severe´ desaturation compared to the patients with ´mild´ desaturation. Before the desaturation, the PSD between the ´mild´ and ´severe´ desaturation group were comparable. Interestingly, when comparing the PSD after the desaturation, we observed a higher delta-band power and lower alpha- and beta-band power in patients with ´severe´ desaturation. To statistically test the observed difference in the PSD after the desaturation between the two groups, we calculated the AUC with 95% confidence intervals (table 14). Figure 22 presents the corresponding normalized PSD plots before and after cerebral desaturation.

frequency	AUC	95%- Confidence Interval
alpha	0.8	[0.4 – 1]
beta	0.8	[0.4 – 1]
delta	0.2	[0 – 0-6]
theta	0.55	[0.15 – 1]

Table 14: AUC of PSD from 10-second-EEG epoch after ´mild´ vs. after ´severe´ desaturation.

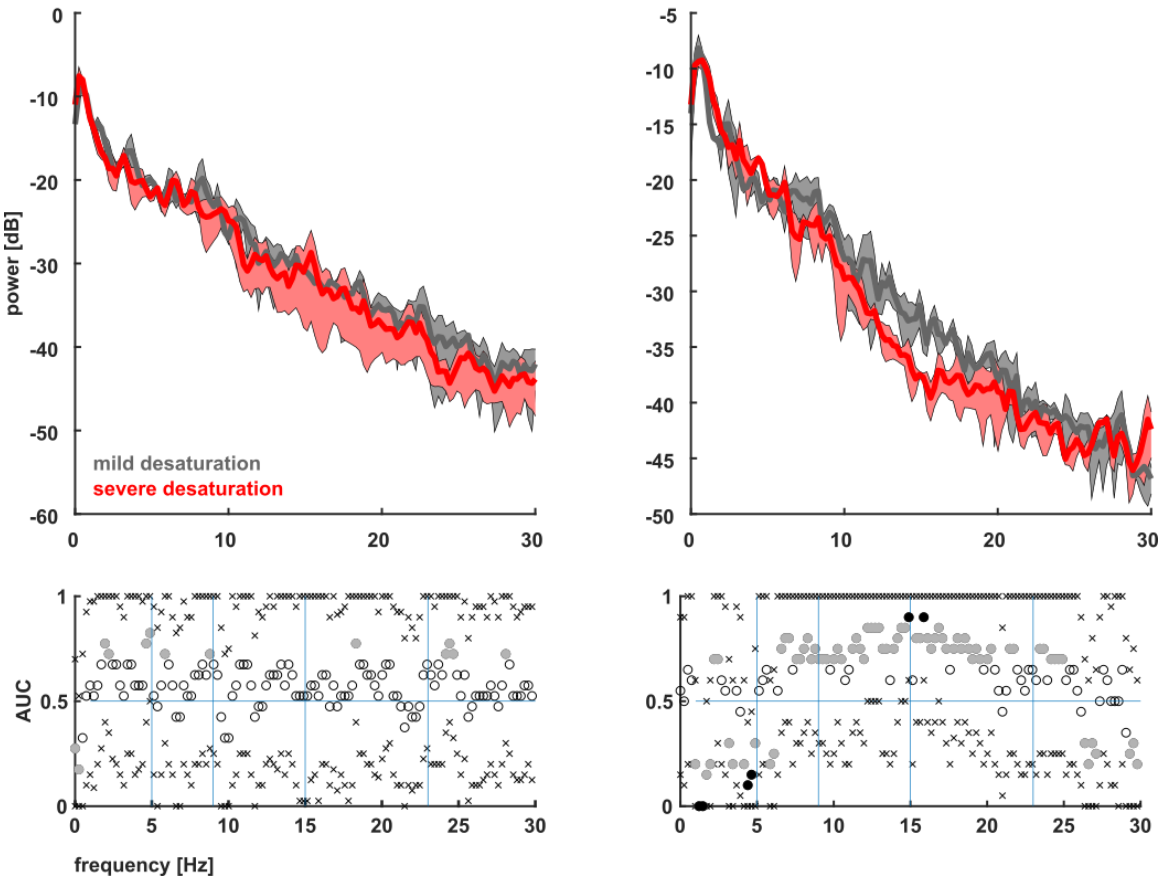

Figure 22: Power spectral density before (left) and after (right) ´mild´ and ´severe´ desaturation.

4. Discussion of our findings

4.1. Elaboration of the analysis method

To conduct pilot investigations regarding saturation related changes of the EEG, a controlled setting is crucial since other intraoperative factors like temperature and MAC also influence the EEG (Levy, 1984; Söhle, 2014; Stein, 2010). In our pre-analyses we found a general decline of amplitudes of the EEG in patients with a temperature below 34°C. Thus, we only included recordings during temperature > 35°C for further analyses. Pre-analyses of the association between NCT index and NIRS revealed both, an increase and a decrease of the NCT index with increasing NIRS, dependent on the concomitant aaMAC values. For the linear model, we therefore controlled for the aaMAC to be within 0.6 - 0.8. The literature suggests that the limits of cerebral autoregulation shift in certain patient groups and that disturbed cerebral autoregulation occurs more often than expected (Hori et al., 2014; C. Lewis et al., 2018; Ono et al., 2012). If intact cerebral autoregulation cannot be guaranteed, changes in the mean arterial pressure may be another influencing factor. Retrospectively, we cannot define or exclude situations of ´impaired autoregulation´. To reduce the influence of cerebral autoregulation mechanisms, we only included data from episodes when the MAP was within 50 - 150 mmHg.

This thesis aims to identify EEG features that are worth further investigations regarding cerebral saturation related changes of the EEG in adults under general anesthesia. Therefore, we performed the analyses in several steps that build on each other. We started with an analysis of the rEEG- a recently developed modification of the aEEG, which is already used in combination with NIRS (Toet, Lemmers, van Schelven, & van Bel, 2006; Variane et al., 2019; Zhang et al., 2012). Only rEEG is described to provide a reasonable estimate of the absolute value of amplitude and to regard lower frequencies (O'Reilly et al., 2012). Because both, the change of amplitudes and the low frequencies, are of particular interest in anesthesia research, we chose to analyze rEEG instead of aEEG. To our knowledge, the rEEG in combination with NIRS has not been investigated in adults undergoing general anesthesia yet. Besides rEEG, we wanted to analyze EEG parameters, which are being researched in terms of anesthesia monitoring. Like the rEEG, the EEG power takes amplitudes into account, and is incorporated into our analyses by the PSD and the SpEn. The SpEn is used in

commercially available EEG modules already (Matthias Kreuzer et al., 2020). Finally, we investigated changes of the permutation entropy, a parameter of strong interest in current anesthesia research. Although the EEG and its neurological clinical correlates are not linear phenomena, intraoperative monitors provide information derived from the raw EEG signal on a linear scale. Likewise, the NIRS signal is displayed on a linear scale. Thus, we chose the linear model to find out whether there is an observable positive or negative relation between several different EEG parameters and the NIRS signal. We assume the linear model to be an appropriate method to begin with analyzing the link between different EEG parameters and cerebral saturation in our data set.
To present our research interest to the international public, we performed an additional analysis of individual cases (Klinker S. D., 2020). These cases were selected visually and a ´mild´ and ´severe´ desaturation group was defined. The analysis includes the SpEn of the EEG, a parameter implemented in commercially available intraoperative monitors. It also includes the PSD of the EEG, a parameter integrated in index calculation of intraoperative monitors. As our preceding linear model on the rEEG revealed saturation related changes of the EEG amplitudes, PSD analysis served as another approach to regard EEG amplitudes. Both, the SpEn and the PSD were calculated from the raw EEG, which is still considered as ´gold standard´ in monitoring brain activity.

4.2. Integration in the literary context

The rEEG analyses revealed a link between the cerebral saturation and the amplitudes of different EEG frequencies. This finding justifies the use of rEEG not only in pediatrics but also in adults undergoing general anesthesia. We found that the change of the EEG amplitudes with changing NIRS under controlled conditions is not uniform, i.e. it was different within different frequencies and within different parameters of the rEEG. Reduced cerebral oxygen delivery is described to result in a decrease in amplitudes of higher frequency alpha (8 - 12 Hz) and beta (12 - 20 Hz) waves and an increase in amplitudes of lower frequency theta (4 - 8 Hz) or delta (1 - 4 Hz) waves (C. Lewis et al., 2018). This is also considered as ´general slowing´ of the EEG (Söhle, 2014). As a deepening of anesthesia can also result in ´general slowing´, more profound analyses of the saturation related changes in amplitudes can be helpful. Our rEEG analyses allow a further specification of the changes in amplitudes. In accordance with the literature, we observed a decrease of both, the UM and LM, of amplitudes in the alpha and beta

frequency with decreasing NIRS signal. In the lower frequencies the bandwidth increased with decreasing NIRS signal, as either the UM or the LM changes. Remember that we did not define ´cerebral ischemia´ or ´critical desaturation´ for our investigation on rEEG changes in relation to cerebral saturation. Our study should instead provide information about the median rEEG parameter that occurs with a certain NIRS value and reveal possible parameter trends associated with NIRS.

As we observed an influence of the NIRS level on the amplitudes, and as amplitudes are considered in terms of EEG power, we analyzed the absolute and relative power of the EEG with the same linear model. As the observed change was different within the different frequency bands, we applied the linear model for each frequency separately. In literature, decreased power in faster frequency bands (alpha and beta) and increased power in slower frequency bands (delta and theta) were described with reduction in brain metabolism (Foreman B., 2012). Changes in relative delta power due to cerebral ischemia were described for patients receiving propofol (Foreman B., 2012). Moreover, changes in relative delta power were described to correlate well with CBF and cerebral metabolism during focal ischemia (Foreman B., 2012). In our analyses of the power spectrum parameters, we found a statistically significant reduction of relative alpha band power with decreasing NIRS value. Concerning relative delta power, we found a non-significant increase with decreasing NIRS, conversely to what Foreman et al. describe about the change of relative delta power. In line with our findings, a review from 1998 states that an increase of delta band power could represent ischemia in the EEG (Ira J. Rampil, 1998). For other frequency bands we could not identify a statistically significant change in absolute or relative power. This difference of our findings compared to other published results could be explained by the fact that we did not investigate changes in relation to ´cerebral ischemia´, but in relation to a certain range of observed NIRS values. Most of these observed NIRS values lay in a range in which sufficient cerebral oxygenation can be assumed. It is also necessary to differentiate ´changes of cerebral metabolism´ from ´changes of the NIRS level´. Hence, our findings may only be comparable to the literature in a limited fashion. However, the investigation of individual cases of ´mild´ or ´severe´ cerebral desaturation revealed two different ´post-desaturation´ PSD patterns. In the ´severe´ cerebral desaturation group the delta-band power was higher, whereas the alpha- and beta-band power was lower, compared to the ´mild´ desaturation group. The electrophysiological change during ´severe´ cerebral desaturation corresponds to the concept of general slowing in the raw EEG during ischemia. The ´pre-desaturation´ PSD was comparable between both groups. This finding suggests that cerebral desaturation can influence PSD analyses. In 1989

already, an increase of relative delta and theta power as well as a decrease of relative alpha and beta power was described with decreasing regional CBF (Nagata, Tagawa, Hiroi, Shishido, & Uemura, 1989). If a reduction in cerebral metabolism is associated with the term of ischemia, our definition of cerebral desaturation can be related to it as well. Then, our PSD analyses support Foreman`s and Nagata`s description of changes of the EEG power.

The linear model then revealed an increase of the NCT index with increasing NIRS. Dennhardt et al. described an inverse correlation of the NCT index and NIRS signal in children under sevoflurane anesthesia during CPB (Dennhardt et al., 2018). This negative correlation was explained by the fact that they did not control for the temperature and that hypothermia alone can decrease the NCT index and increase the NIRS value. In our linear model, we only included values observed during normothermia (> 35°C) and observed a positive correlation. Besides the NCT monitor, also BIS guided monitoring integrates processed EEG analyses for intraoperative monitoring. A study of Stein et al. suggests a negative association between the BIS index and mixed venous oxygen saturation in adults, which could only be observed during hypothermia < 34.1°C (Stein, 2010). In four case reports Couture et al. describe the various possibilities of interaction between the cerebral NIRS level and another pEEG index, the Patient State index (PSI, Masimo, Irvine). The study describes the change of both signals in the same direction as well as in the opposite direction, depending on the cause of the change. The related algorithm is provided in the Appendix (Couture, Deschamps, & Denault, 2019).

Entropy measures of the EEG may provide information on the state of anesthesia. SpEn is implemented in commercially available EEG monitors to reflect the hypnotic level of anesthesia (H. Viertiö-Oja, 2004). Perhaps a change in cerebral saturation also influences entropic parameters applied to the EEG. We therefore investigated the relationship between the SpEn and the NIRS level using the linear model and could not observe a statistically significant relationship. However, the investigation of individual cases of NIRS decrease, revealed a change in the SpEn. This change was not uniform, i.e. the SpEn tended to increase when the NIRS value decreases below 50%, whereas the SpEn decreased when the NIRS decrease was not below 50%. Our results suggest that the influence on entropic parameters may be biphasic and not captured by linear models.

Finally, we investigated the relationship between PEn and cerebral oxygenation using a linear model and could not find a statistically significant relationship. PEn has been described as ´state of the art´ parameter to distinguish consciousness from

unconsciousness during general anesthesia (Jordan, 2008). PEn is proposed to be robust against signal artifacts and is until now mainly used as a ´research parameter´ in anesthesia. A prospective study on the effect of sevoflurane anesthesia, evaluated with PEn, found a decreased frontal and thalamocortical neuronal connectivity (Ranft et al., 2016). This study also found reduced anterio-posterior connectivity and reduced cortical information processing, evaluated with fMRI. We took this study into account, as it investigated the effect of another halogenated ether on the brain and as it investigated EEG changes simultaneously to a metabolic parameter. A recent study indicates that the PEn can increase with increasing age (Matthias Kreuzer et al., 2020). To regard a modern parameter of anesthesia research and to possibly detect a saturation related influence, we analyzed the PEn, using our linear model.

4.3. Proposed mechanisms

The increase of amplitudes of higher frequencies (alpha and beta) with increased NIRS signal could be explained by enhanced intrinsic activity of neurons of the thalamocortical circuits (E R. John & Prichep, 2005). This finding could be limited to higher frequencies as they are described to react on reduced CBF earlier than lower frequencies (Foreman B., 2012). Especially the alpha frequency is described to represent intrinsic thalamocortical activity, which may be more susceptible to changes in cerebral oxygenation. A change of both, the UM and LM of the rEEG indicates, that both, highly and less synchronous oscillations of neurons, may change with cerebral saturation.

The narrowing of the bandwidth of amplitudes of lower frequencies (delta and theta) results from either the decrease of the UM (delta) or increase of the LM (theta). Neural oscillatory activity in the delta frequency is described to be generated by deprived cortical neurons, whereas theta activity is generated in the limbic system (E. R. John, 2005). A narrowing in the bandwidth could indicate more regularity of the amplitudes of oscillations generated by neurons in the limbic system or in intracortical networks. Further, this regularity might be enhanced by a change in cerebral metabolism. The change of metabolism may be captured by NIRS. Why exactly the UM or LM or both of a certain frequency changes with a change of NIRS, cannot be explained satisfactorily by our investigations. However, we assume that rEEG analyses can help to find saturation related changes of the EEG under general anesthesia in adults.

We observed that the magnitude of amplitudes as investigated with the rEEG changed with NIRS fluctuations, however, the band power did not, except for alpha. That this

finding was limited on the alpha frequency may be explained by increased susceptibility towards changes in cerebral saturation compared to other frequency bands (Söhle, 2014). It may also be related to the median age (67 years) as recent studies indicate an influence of age on the alpha frequency. For example, the decrease of power during general anesthesia is described to be more obvious in the alpha frequency band than in lower frequencies in the elderly (Purdon, Pavone, et al., 2015). Hight et al. could find a slowing of alpha oscillation with increasing age (Hight, Voss, Garcia, & Sleigh, 2017). Concerning the relative alpha power, no significant impact of age was found in another study (Matthias Kreuzer et al., 2020). Another reason for the finding exclusively in the alpha frequency could also be the selected period of recordings. We controlled for the aaMAC to be within 0.6-0.8, however we can´t ensure that this targeted anesthetic concentration has been stable or just been reached. If it has just been reached by increasing the anesthetic concentration, an initial increase and subsequent decrease in alpha power could have been provoked (Hight et al., 2017).

The change of amplitudes, or the change of power, may be related to a brain state resembling ´cognitive unbinding´ in the anesthetized brain. To investigate this, it would be helpful to include oscillations in the y-frequency around 40 Hz, which we did not include (Mashour, 2004). Until now only the BIS monitor is suggested to reflect y-band desynchronization (Mashour, 2004).

We could observe a linear relationship between the NCT index and the NIRS signal. Like other pEEG monitors, the NCT monitor should help to evaluate adequate level of hypnosis. A decreasing anesthetic concentration should lead to an increase in the index. A decreasing concentration of the anesthetic could also lead to a decrease in cerebral oxygenation - due to an increased cerebral oxygen consumption. On the other hand, a reduced effect of the anesthetics could also lead to an increase in the cerebral oxygenation and the NIRS level - due to cerebral vasodilatation caused by neurovascular uncoupling mechanism or volatile anesthetics. To differentiate between the possible scenarios, a combination of pEEG and NIRS, as suggested by Couture et al. needs to be further investigated. To improve the evaluation of the anesthetic level by EEG monitors, taking the influence of cerebral saturation on the pEEG into account, could be useful. To investigate neurovascular uncoupling mechanism through general anesthesia, functional imaging or the combination of EEG and functional NIRS could be helpful (Chiarelli et al., 2017; Palanca et al., 2009; Palanca et al., 2015). Our approach does not allow to draw conclusions on neurovascular mechanisms.

The investigation of individual cases of NIRS decrease and SpEn revealed a biphasic change of SpEn. SpEn tended to increase when the NIRS value decreased below 50%,

whereas it decreased when the NIRS decrease was not below 50%. An increase of SpEn can also reflect a more profound hypnotic level of anesthesia. In our analyses, the SpEn increase might still reflect a more profound hypnotic level, however not due to anesthesia but to cerebral desaturation. The increase of the entropy in the spectrum, indicative for more irregularity in the EEG, might reflect a state of ´neuronal arousal´ due to beginning cerebral desaturation. Another explanation of our finding would be, that NIRS decreases due to increased cerebral metabolism, thus due to a decline of the hypnotic component of anesthesia. In this case, SpEn indeed reflected this decline of hypnosis, however only until a certain extend of desaturation, i.e. only for desaturation not below 50% NIRS.

4.4. Limitations

Due to the retrospective study design, our results should be interpreted with caution. In addition, the data set originates from cardiac surgery. This means that both, the patient-related comorbidities and the intervention-related risk factors may be above average. On the one hand, correlations between EEG parameters and the NIRS level could remain undetected, on the other hand, they cannot be automatically transferred to other patient groups. To minimize intervention-related distortions of the results, particularly by the CPB, we have included only the period before initiation of CPB. At the same time, this means that we cannot display and analyze the entire general anesthetic. We only included isoflurane anesthesia, however the chosen agent for providing general anesthesia itself could affect EEG frequency bands and amplitudes (Purdon, Sampson, et al., 2015). Another limitation of EEG interpretation could be the fact that we did not control for age, which can also influence the EEG (Matthias Kreuzer et al., 2020; Purdon, Pavone, et al., 2015), nor for the predominance of male patients. Maybe our linear model does not capture a certain relationship, because it is not linear, or because the relationship would refer to specific sequences of the recording. Due to the retrospective approach of the investigation, we chose to present the median observed EEG parameter during the whole analyzed period. This means, we did not account for specific events, limited on short sequences of the analyzed period. For example, in the linear model on entropic features of the EEG, we could not observe a statistically significant relationship for neither PEn nor SpEn and the NIRS signal. However, in the analyses of specific cases we indeed observed an interesting link between the NIRS signal and the SpEn. Because of the assumed limitations, we did not analyze further entropic parameters, like

the approximate entropy with the linear model. Another limitation of our study is that we cannot verify the basis of the delivered NIRS value. It depends on many factors, i.e. local oxygen extraction and metabolism or the cerebral blood flow, which again depends on many factors, i.e. CO_2 content, anesthetics, MAP or vasoreactive processes. Therefore, we cannot contribute to the debate on a relative or absolute NIRS threshold for intervention. We also did not intend to define or analyze ´cerebral ischemia´ which might make a comparison with other studies on the NIRS signal difficult.

4.5. Relevance of our analyses

With our analyses we could show that NIRS determined cerebral saturation seems to influence the EEG. Current EEG-based monitoring is kind of a one-fits-all-approach. There is wide agreement that monitors should consider patient or procedural related differences, such as age, cognitive status, anesthetic drug, and metabolic differences. These differences might play a significant role in computing and developing specific EEG algorithms, i.e. specific for the level of anesthesia or cerebral saturation. Already in 1998, Rampil nicely expressed, that the aim of EEG quantification should be to find the ´needle´ in the ´electric haystack´, the respective parameter that helps to evaluate certain pharmacological or physiological mechanism (Ira J. Rampil, 1998). In search for the ´needle´, various parameters of the EEG have been investigated. Metaphorically spoken, if you want to find the needle to evaluate ´level of anesthesia´, you should try to exclude any other influences on this needle. Equally, if you want to find the needle to evaluate ´cerebral ischemia´. Figure 23 helps to illustrate different objectives and interconnections in the context of analyzing the ´EEG haystack´. In 2020 a research group in Gothenburg has published their study protocol for developing a method to detect cerebral ischemia in unconscious patients by analyzing changes in heart rate variability, the NIRS signal and the EEG (Block et al., 2020). Future, prospective studies are required to answer if and how cerebral saturation influences different parameters of the EEG. For any investigation of saturation related changes in the EEG, we recommend to control for the temperature and the anesthetic drug concentration. We suggest that rEEG analyses can help to find saturation related EEG changes under general anesthesia in adults. In terms of rEEG analyses, we emphasize the need to separate between the frequency bands. We further suggest to include high frequency ranges, like the y-band. The impact of cerebral saturation on the amplitudes of the EEG may also play a role in analyses of the power, the peak frequency or the approximate entropy. In

terms of entropy analyses, the influence of cerebral saturation might be subtle, non-linear and depend on the dynamic of the NIRS change, i.e. the extend or temporal course. Even if it was retrospective, not controlled and within a cardiac patient cohort, which might be exposed to higher intraoperative risk, we found saturation related changes of the EEG. These changes could possibly influence EEG based evaluation of level of anesthesia. For more profound analyses of cerebral saturation related influences on specific EEG parameters we suggest to conduct prospective, randomized controlled studies in a representative patient cohort, i.e. not cardiac patients.

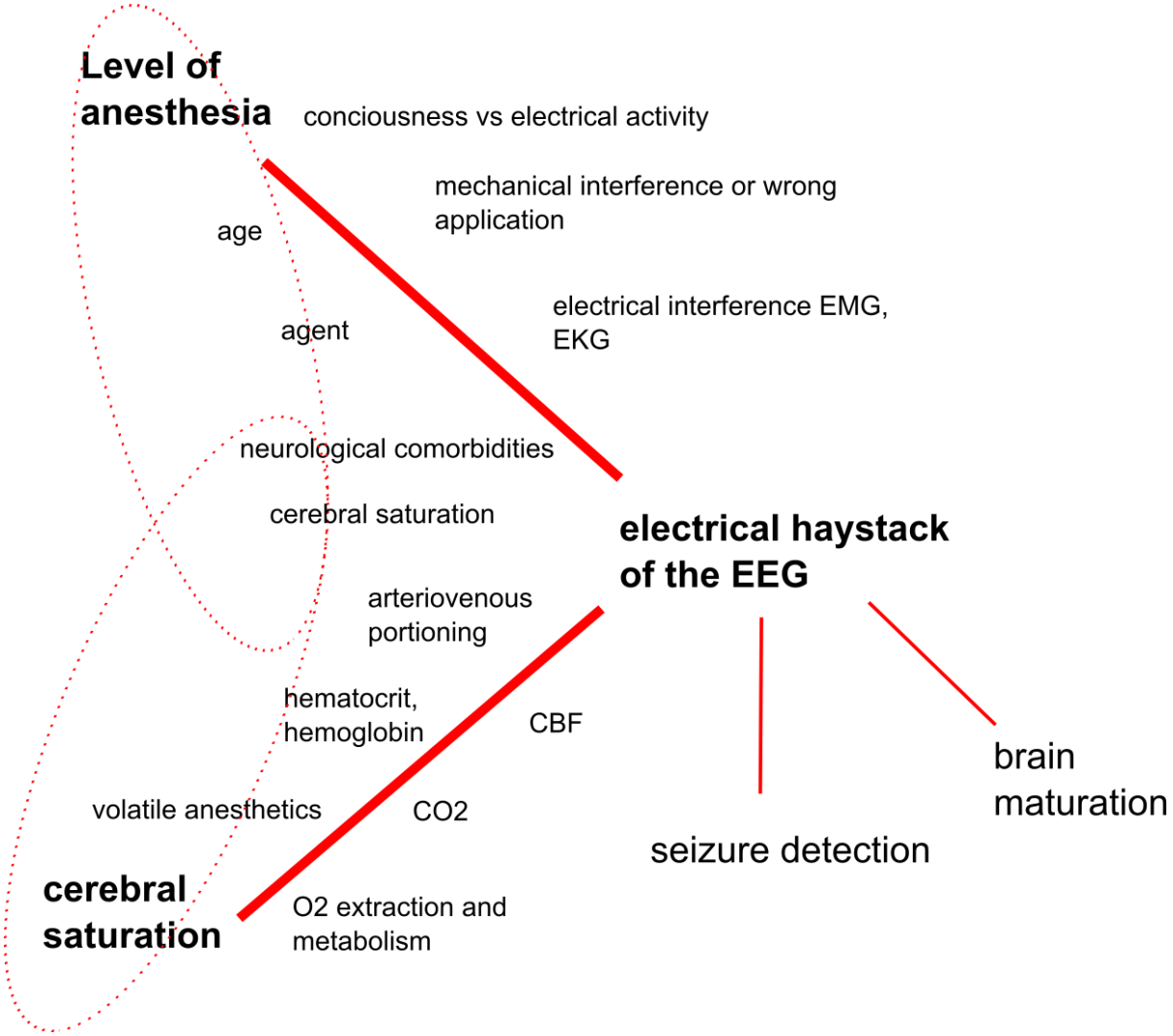

Figure 23: Illustration of the objectives and connections in the context of EEG analyses.

5. References

Akeju, O., Westover, M. B., Pavone, K. J., Sampson, A. L., Hartnack, K. E., Brown, E. N., & Purdon, P. L. (2014). Effects of sevoflurane and propofol on frontal electroencephalogram power and coherence. *Anesthesiology, 121*(5), 990-998. doi:10.1097/aln.0000000000000436

al Naqeeb, N., Edwards, A. D., Cowan, F. M., & Azzopardi, D. (1999). Assessment of neonatal encephalopathy by amplitude-integrated electroencephalography. *Pediatrics, 103*(6 Pt 1), 1263-1271. doi:10.1542/peds.103.6.1263

Aldecoa, C., Bettelli, G., Bilotta, F., Sanders, R. D., Audisio, R., Borozdina, A., Jones C., Kehlet H., MacLullich A., Radtke F., Riese F., Slooter A.J.C., Veyckemans F., Kramer S., Neuner B., Weiss B., Spies, C. D. (2017). European Society of Anaesthesiology evidence-based and consensus-based guideline on postoperative delirium. *Eur J Anaesthesiol, 34*(4), 192-214. doi:10.1097/eja.0000000000000594

Aryeh, S. (2018). Brain Monitoring and the Depth of Anesthesia: Another Goldilocks Dilemma. *Anesth Analg*. doi:10.1213/ANE.0000000000002383

Asgari, S., Moshirvaziri, H., Scalzo, F., & Ramezan-Arab, N. (2018). Quantitative measures of EEG for prediction of outcome in cardiac arrest subjects treated with hypothermia: a literature review. *J Clin Monit Comput, 32*(6), 977-992. doi:10.1007/s10877-018-0118-3

Bandt, C., & Pompe, B. (2002). Permutation entropy: a natural complexity measure for time series. *Phys Rev Lett, 88*(17), 174102. doi:10.1103/PhysRevLett.88.174102

Bennett, M. J., Weatherall, M., Webb, G., Dudnikov, S. F., & Lloyd, C. T. (2015). The impact of haemodilution and bypass pump flow on cerebral oxygen desaturation during cardiopulmonary bypass-A comparison of two systems of cardiopulmonary bypass. *Perfusion, 30*(5), 389-394. doi:10.1177/0267659114548256

Block, L., El-Merhi, A., Liljencrantz, J., Naredi, S., Staron, M., & Odenstedt Hergès, H. (2020). Cerebral ischemia detection using artificial intelligence (CIDAI)-A study protocol. *Acta Anaesthesiol Scand*. 00,1–8. doi:10.1111/aas.13657

Braz, L. G. (2009). Mortality in Anesthesia: A Systematic Review. *Clinics*. doi:10.1590/S1807-59322009001000011

Brown, E. N., Lydik R. (2010). General Anesthesia, Sleep, and Coma. *The New England Journal of Medicine, 363*, 2638-2650.

Bruhn, J., Lehmann L.E., Röpcke, H., Bouillon, T. W., Hoeft A. (2001). Shannon Entropy Applied to the Measurement of the EEG effects of desflurane. *Anesthesiology, 95, 30–5.*

Bruhn, J., Myles, P. S., Sneyd, R., & Struys, M. M. (2006). Depth of anaesthesia monitoring: what's available, what's validated and what's next? *Br J Anaesth, 97*(1), 85-94. doi:10.1093/bja/ael120

Caicedo, A., Thewissen, L., Smits, A., Naulaers, G., Allegaert, K., & Van Huffel, S. (2016). Changes in Oxygenation Levels Precede Changes in Amplitude of the EEG in Premature Infants. *Adv Exp Med Biol, 923*, 143-149. doi:10.1007/978-3-319-38810-6_19

Calderon-Arnulphi, M., Alaraj, A., Amin-Hanjani, S., Mantulin, W. W., Polzonetti, C. M., Gratton, E., & Charbel, F. T. (2007). Detection of cerebral ischemia in neurovascular surgery using quantitative frequency-domain near-infrared spectroscopy. *J Neurosurg, 106*(2), 283-290. doi:10.3171/jns.2007.106.2.283

Casati, A., Fanelli, G., Pietropaoli, P., Proietti, R., Tufano, R., Danelli, G., Fierro, G., De Cosmo, G., Servillo, G. (2005). Continuous monitoring of cerebral oxygen saturation in elderly

patients undergoing major abdominal surgery minimizes brain exposure to potential hypoxia. *Anesth Analg, 101*(3), 740-747, table of contents. doi:10.1213/01.ane.0000166974.96219.cd

Chan, M. T. V., Hedrick, T. L., Egan, T. D., García, P. S., Koch, S., Purdon, P. L., Ramsay , M. A., Miller, T.E., Gan, T. J. (2020). American Society for Enhanced Recovery and Perioperative Quality Initiative Joint Consensus Statement on the Role of Neuromonitoring in Perioperative Outcomes: Electroencephalography. *Anesth Analg, 130*(5), 1278-1291. doi:10.1213/ane.0000000000004502

Chiarelli, A. M., Zappasodi, F., Di Pompeo, F., & Merla, A. (2017). Simultaneous functional near-infrared spectroscopy and electroencephalography for monitoring of human brain activity and oxygenation: a review. *Neurophotonics, 4*(4), 041411. doi:10.1117/1.NPh.4.4.041411

Choi, H.-I., Noh, G.-J., & Shin, H.-C. (2020). Measuring the Depth of Anesthesia Using Ordinal Power Spectral Density of Electroencephalogram. *IEEE Access, 8*, 50431-50438. doi:10.1109/access.2020.2980370

Cohen, B. A., & Sances, A., Jr. (1977). Stationarity of the human electroendephalogram. *Med Biol Eng Comput, 15*(5), 513-518. doi:10.1007/bf02442278

Colombo, M. A., Napolitani, M., Boly, M., Gosseries, O., Casarotto, S., Rosanova, M., Brichant, J.F., Boveroux, P., Rex, S., Laureys, S., Massimini, M., Chieregato, A., Sarasso, S. (2019). The spectral exponent of the resting EEG indexes the presence of consciousness during unresponsiveness induced by propofol, xenon, and ketamine. *Neuroimage, 189*, 631-644. doi:10.1016/j.neuroimage.2019.01.024

Couture, E. J., Deschamps, A., & Denault, A. Y. (2019). Patient management algorithm combining processed electroencephalographic monitoring with cerebral and somatic near-infrared spectroscopy: a case series. *Can J Anaesth, 66*(5), 532-539. doi:10.1007/s12630-019-01305-y

Dagal, A., & Lam, A. M. (2009). Cerebral autoregulation and anesthesia. *Curr Opin Anaesthesiol, 22*(5), 547-552. doi:10.1097/ACO.0b013e32833020be

Dandan, Z. (2008). Cerebral hypoxic ischemia at different cerebral oxygen saturations in piglets: amplitude-integrated EEG study *IEEE EMBS Conference*.

de Vries, L. S., & Hellstrom-Westas, L. (2005). Role of cerebral function monitoring in the newborn. *Arch Dis Child Fetal Neonatal Ed, 90*(3), F201-207. doi:10.1136/adc.2004.062745

Del Rio, R., Ochoa, C., Alarcon, A., Arnaez, J., Blanco, D., & Garcia-Alix, A. (2016). Amplitude Integrated Electroencephalogram as a Prognostic Tool in Neonates with Hypoxic-Ischemic Encephalopathy: A Systematic Review. *Plos One, 11*(11), e0165744. doi:10.1371/journal.pone.0165744

Denault André, Deschamps, A., Murkin, J. M. (2007). A proposed algorithm for the intraoperative use of cerebral near-infrared spectroscopy. Seminars in Cardiothoracic and Vascular Anesthesia Volume 11 Number 4 December 2007 274-281, 10.1177/1089253207311685

Dennhardt, N., Beck, C., Boethig, D., Heiderich, S., Horke, A., Tiedge, S., Böhne, M., Sümpelmann, R. (2018). Impact of temperature on the Narcotrend Index during hypothermic cardiopulmonary bypass in children with sevoflurane anesthesia. *Perfusion, 33*(4), 303-309. doi:10.1177/0267659117746234

Douds, M. T., Straub, E. J., Kent, A. C., Bistrick, C. H., & Sistino, J. J. (2014). A systematic review of cerebral oxygenation-monitoring devices in cardiac surgery. *Perfusion, 29*(6), 545-552. doi:10.1177/0267659114544713

Drohan, C. M., Cardi, A. I., Rittenberger, J. C., Popescu, A., Callaway, C. W., Baldwin, M. E., & Elmer, J. (2018). Effect of sedation on quantitative electroencephalography after cardiac arrest. *Resuscitation, 124*, 132-137. doi:10.1016/j.resuscitation.2017.11.068

Edmonds, G. (2004). Cerebral Oximetry for Cardiac and vascular surgery, in , 2004. *Seminars in Cardiothoracic and vascular Anesthesia 8*, 147-166.

Fahy B.G., C. D. F. (2017). The Technology of Processed Electroencephalogram Monitoring Devices for Assessment of Depth of Anesthesia. *Anesth Analg, 126*, 111-117. doi:10.1213/ANE.0000000000002331

Faure, P., & Korn, H. (2001). Is there chaos in the brain? I. Concepts of nonlinear dynamics and methods of investigation. *C R Acad Sci III, 324*(9), 773-793. doi:10.1016/s0764-4469(01)01377-4

Ferrari, M., Mottola, L., Quaresima, V. (2004). Principles, techniques, and limitations of near infrared spectroscopy. *Canadian Journal of Applied Physiology,* 29(4): 463-487

Foreman B., Claasen, J. (2012). *Quantitative EEG for the detection of brain ischemia*. Critical Care 2012, 16:216. doi:10.1186/cc11230

Friberg, H., Westhall, E., Rosén, I., Rundgren, M., Nielsen, N., & Cronberg, T. (2013). Clinical review: Continuous and simplified electroencephalography to monitor brain recovery after cardiac arrest. *17*(4), 233. doi:10.1186/cc12699

Gaskell, A. L., Hight, D. F., Winders, J., Tran, G., Defresne, A., Bonhomme, V., Ras A., Sleigh J.W., Sanders, R. D. (2017). Frontal alpha-delta EEG does not preclude volitional response during anaesthesia: prospective cohort study of the isolated forearm technique. *Br J Anaesth, 119*(4), 664-673. doi:10.1093/bja/aex170

Ghosh, A., Elwell, C., & Smith, M. (2012). Review article: cerebral near-infrared spectroscopy in adults: a work in progress. *Anesth Analg, 115*(6), 1373-1383. doi:10.1213/ANE.0b013e31826dd6a6

Gluckman, P. D., Wyatt, J. S., Azzopardi, D., Ballard, R., Edwards, A. D., Ferriero, D. M., Polin, R.A., Roberston, C. M., Thoresen, M., Whitelaw, A., Gunn, A. J. (2005). Selective head cooling with mild systemic hypothermia after neonatal encephalopathy: multicentre randomised trial.*The Lancet, 365*(9460),663-670. doi:10.1016/s0140-6736(05)17946-x

Goeral, K., Urlesberger, B., Giordano, V., Kasprian, G., Wagner, M., Schmidt, L., Berger, A., Klebermass-Schrehof, K., Olischar, M. (2017). Prediction of Outcome in Neonates with Hypoxic-Ischemic Encephalopathy II: Role of Amplitude-Integrated Electroencephalography and Cerebral Oxygen Saturation Measured by Near-Infrared Spectroscopy. *Neonatology, 112*(3), 193-202. doi:10.1159/000468976

Goeral, K., Urlesberger, B., Giordano, V., Schmidt, L., Weninger, M., Berger, A., Klebermass-Schrehof, K., Olischar, M. (2015). OP78 – 2871: Correlation between NIRS and aEEG in hypothermia treated newborns with hypoxic-ischemic encephalopathy. *European Journal of Paediatric Neurology, 19*. doi:10.1016/s1090-3798(15)30079-9

Guérit JM. Neuromonitoring in the operating room: why, when, and how to monitor? Electroencephalogr Clin Neurophysiol. 1998 Jan;106(1):1-21. doi: 10.1016/s0013-4694(97)00077-1. PMID: 9680160.

Hadolt I, L. G. (2003). Noninvasive assessment of cerebral oxygenation during high altitude trekking in the Nepal Himalayas (2850 - 5600m). *Neurol Res., 25*, 183-188.

Hart, S., M., Buchannan, C. R., J. W. Sleigh. (2009). A failure of M-Entropy™ to correctly detect burst suppression leading to sevoflurane overdosage. *Anaesth Intensive Care, 37*, 1002-1004.

Harrer, M., Waldenberger, F. R., Weiss, G., Folkmann, S., Gorlitzer, M., Moidl, R., & Grabenwoeger, M. (2010). Aortic arch surgery using bilateral antegrade selective cerebral perfusion in combination with near-infrared spectroscopy. *Eur J Cardiothorac Surg, 38*(5), 561-567. doi:10.1016/j.ejcts.2010.03.016

Hentschke, H., & Stüttgen, M. C. (2011). Computation of measures of effect size for neuroscience data sets. *Eur J Neurosci, 34*(12), 1887-1894. doi:10.1111/j.1460-9568.2011.07902.x

Heringlake, M. (2011). Preoperative cerebral oxygen saturation and clinical outcomes in cardiac surgery. *Survey of Anesthesiology*. doi:10.1097/SA.0b013e318229107b10.1097/01.SA.0000399975.56343.0d

Hight, D., Voss, L. J., Garcia, P. S., & Sleigh, J. (2017). Changes in Alpha Frequency and Power of the Electroencephalogram during Volatile-Based General Anesthesia. *Front Syst Neurosci, 11*, 36. doi:10.3389/fnsys.2017.00036

Honan, D., Doherty, D., & Frizelle, H. (2006). A comparison of the effects on bispectral index of mild vs. moderate hypothermia during cardiopulmonary bypass. *Eur J Anaesthesiol, 23*(5), 385-390. doi:10.1017/S0265021505002309

Horan, M., Azzopardi, D., Edwards, A. D., Firmin, R. K., & Field, D. (2007). Lack of influence of mild hypothermia on amplitude integrated-electroencephalography in neonates receiving extracorporeal membrane oxygenation. *Early Hum Dev, 83*(2), 69-75. doi:10.1016/j.earlhumdev.2006.05.004

Hori, D., Brown, C., Ono, M., Rappold, T., Sieber, F., Gottschalk, A., Neufeld, K. J., Gottesman, R., Adachi, H., Hogue, C. W. (2014). Arterial pressure above the upper cerebral autoregulation limit during cardiopulmonary bypass is associated with postoperative delirium. *Br J Anaesth, 113*(6), 1009-1017. doi:10.1093/bja/aeu319

Jobsis. (1977). Noninvasive, infrared monitoring of cerebral and myocardial oxygen sufficiency and circulatory parameters. *science*.

John, E. R. (2005). The anesthetic cascade - A theory of how anesthesia suppresses consciousness. *Anesthesiology, 102*, 447-471.

John, E R., & Prichep, Leslie S. (2005). The Anesthetic Cascade: A Theory of How Anesthesia Suppresses Consciousness. *Anesthesiology, 102*(2), 447-471. doi:10.1097/00000542-200502000-00030

Jordan, D. S. G. K. E. (2008). Electroencephalographic Order Pattern Analysis for the Separation of Consciousness and Unconsciousness. *Anesthesiology, 109*, 1014-1022.

Joshi, B., Brady, K., Lee, J., Easley, B., Panigrahi, R., Smielewski, P., Czosnyka, M., Hogue, C. W. Jr. (2010). Impaired autoregulation of cerebral blood flow during rewarming from hypothermic cardiopulmonary bypass and its potential association with stroke. *Anesth Analg, 110*(2), 321-328. doi:10.1213/ANE.0b013e3181c6fd12

Kaiser HA, Hirschi T, Sleigh C, Reineke D, Hartwich V, Stucki M, Rummel C, Sleigh J, Hight D. Comorbidity-dependent changes in alpha and broadband electroencephalogram power during general anaesthesia for cardiac surgery. Br J Anaesth. 2020 Oct;125(4):456-465. doi: 10.1016/j.bja.2020.06.054. Epub 2020 Jul 31. PMID: 32747077.

Kertai, M. D., Whitlock, E. L., Avidan, M. S. (2012). Brain monitoring with electroencephalography and the electroencephalogram-derived bispectral index during cardiac surgery. *Anesth Analg, 114*(3), 533-546. doi:10.1213/ANE.0b013e31823ee030

Klinker S. D., K. H., Hight D., Schneider G., Kreuzer M. (2020). Influence of Cerebral Desaturation on the Spectral Entropy of the Electroencephalogram (EEG). *European Journal of Anaesthesiology, 37* (Abstracts Programme), 186.

Kreuer, S., & Wilhelm, W. (2006). The Narcotrend monitor. *Best Practice & Research Clinical Anaesthesiology, 20*(1), 111-119. doi:10.1016/j.bpa.2005.08.010

Kreuzer, M., Kochs, E. F., Schneider, G., Jordan, D. (2014). Non-stationarity of EEG during wakefulness and anaesthesia: advantages of EEG permutation entropy monitoring. *J Clin Monit Comput, 28*(6), 573-580. doi:10.1007/s10877-014-9553-y

Kreuzer, M., Stern, M. A., Hight, D., Berger, S., Schneider, G., Sleigh, J. W., García, P. S. (2020). Spectral and Entropic Features Are Altered by Age in the Electroencephalogram in Patients under Sevoflurane Anesthesia. *Anesthesiology, 132*(5), 1003-1016. doi:10.1097/aln.0000000000003182

Henson, L. C., Calalang, C., Temp, J. A., Ward, D.S. (1998). Accuracy of a cerebral oximeter in healthy volunteers under conditions of isocapnic hypoxia, Anesthesiology. Jan;88(1):58-65.doi: 10.1097/00000542-199801000-00011

Levy. (1984). Quant EEG analysis during Hypothermia and CPB. *Anesthesiology*.

Lewis, C., Parulkar, S. D., Bebawy, J., Sherwani, S., & Hogue, C. W. (2018). Cerebral Neuromonitoring During Cardiac Surgery: A Critical Appraisal With an Emphasis on Near-Infrared Spectroscopy. *J Cardiothorac Vasc Anesth, 32*(5), 2313-2322. doi:10.1053/j.jvca.2018.03.032

Lewis, C. B., & Adams, N. (2020). Phenobarbital. In *StatPearls*. Treasure Island (FL).

Li, G. (2009). Epidemiology of Anesthesia-related Mortality in the United States, 1999-2005. *Anesthesiology*.

Mashour, George A. (2004). Consciousness Unbound: Toward a Paradigm of General Anesthesia. *Anesthesiology, 100*(2), 428-433. doi:10.1097/00000542-200402000-00035

Michels, P., Bräuer, A., Bauer, M. *et al.* Neurophysiologisches Monitoring bei operativen Eingriffen. *Anaesthesist* **66,** 645–659 (2017). https://doi.org/10.1007/s00101-017-0356-7

Moerman, A., Vanbiervliet, V. M., Van Wesemael, A., Bouchez, S. M., Wouters, P., De Hert, S. G., (2015). Assessment of Cerebral Autoregulation patterns with NIRS during pharma-induced pressure changes. *Anesthesiology*. 123:327-35

Moerman, A., Wouters, P., (2010). Near-infrared spectroscopy (NIRS) monitoring in contemporary anesthesia and critical care. *Acta Anaesthesia Belgica*. 61, 185-194

Moerman, A., Vandenplas, G., Bove, T., Wouters, P. F., & De Hert, S. G. (2013). Relation between mixed venous oxygen saturation and cerebral oxygen saturation measured by absolute and relative near-infrared spectroscopy during off-pump coronary artery bypass grafting. *Br J Anaesth, 110*(2), 258-265. doi:10.1093/bja/aes375

Muniz, C. F., Shenoy, A. V., O'Connor, K. L., Bechek, S. C., Boyle, E. J., Guanci, M. M., Tehan, T. M., Zafar, S. F., Cole, A. J., Patel, A. B., Westover, M. B., Rosenthal, E. S. (2016). Clinical Development and Implementation of an Institutional Guideline for Prospective EEG Monitoring and Reporting of Delayed Cerebral Ischemia. *J Clin Neurophysiol, 33*(3), 217-226. doi:10.1097/WNP.0000000000000281

Murkin, J. M. (2009). NIRS A Standard of Care for CPB vs an Evolving standard for selective cerebral perfusion. *The Journal of ExtraCorporeal Technology*. 41:11–14

Murkin, J. M. (2011). cerebral oximetry monitoring the brain as the index organ. *Anesthesiology*. 114: 12–3

Murkin, J. M., Adams, S. J., Novick, R. J., Quantz, M., Bainbridge, D., Iglesias, I., Cleland, A., Schaefer, B., Irwin, B., Fox, S. (2007). Monitoring brain oxygen saturation during coronary bypass surgery: a randomized, prospective study. *Anesth Analg, 104*(1), 51-58. doi:10.1213/01.ane.0000246814.29362.f4

Murkin, J. M., & Arango, M. (2009). Near-infrared spectroscopy as an index of brain and tissue oxygenation. *Br J Anaesth, 103 Suppl 1*, i3-13. doi:10.1093/bja/aep299

Nagata, K., Tagawa, K., Hiroi, S., Shishido, F., & Uemura, K. (1989). Electroencephalographic correlates of blood flow and oxygen metabolism provided by positron emission tomography in patients with cerebral infarction. *Electroencephalogr Clin Neurophysiol, 72*(1), 16-30. doi:10.1016/0013-4694(89)90027-8

Nagdyman, N., Ewert, P., Peters, B., Miera, O., Fleck, T., & Berger, F. (2008). Comparison of different near-infrared spectroscopic cerebral oxygenation indices with central venous and jugular venous oxygenation saturation in children. *Paediatr Anaesth, 18*(2), 160-166. doi:10.1111/j.1460-9592.2007.02365.x

Nashef, S. A., Roques, F., Sharples, L. D., Nilsson, J., Smith, C., Goldstone, A. R., & Lockowandt, U. (2012). EuroSCORE II. *Eur J Cardiothorac Surg, 41*(4), 734-744; discussion 744-735. doi:10.1093/ejcts/ezs043

Nickalls, R. W., & Mapleson, W. W. (2003). Age-related iso-MAC charts for isoflurane, sevoflurane and desflurane in man. *Br J Anaesth, 91*(2), 170-174. doi:10.1093/bja/aeg132

Nielsen, H. B. (2014). Systematic review of near-infrared spectroscopy determined cerebral oxygenation during non-cardiac surgery. *Front Physiol, 5*, 93. doi:10.3389/fphys.2014.00093

O'Reilly, D., Navakatikyan, M. A., Filip, M., Greene, D., & Van Marter, L. J. (2012). Peak-to-peak amplitude in neonatal brain monitoring of premature infants. *Clin Neurophysiol, 123*(11), 2139-2153. doi:10.1016/j.clinph.2012.02.087

Ono, M., Joshi, B., Brady, K., Easley, R. B., Zheng, Y., Brown, C., Baumgartner, W., Hogue, C. W. (2012). Risks for impaired cerebral autoregulation during cardiopulmonary bypass and postoperative stroke. *Br J Anaesth, 109*(3), 391-398. doi:10.1093/bja/aes148

Palanca, B. J., Mashour, G. A., & Avidan, M. S. (2009). Processed electroencephalogram in depth of anesthesia monitoring. *Curr Opin Anaesthesiol, 22*(5), 553-559. doi:10.1097/ACO.0b013e3283304032

Palanca, B. J., Mitra, A., Larson-Prior, L., Snyder, A. Z., Avidan, M. S., & Raichle, M. E. (2015). Resting-state Functional Magnetic Resonance Imaging Correlates of Sevoflurane-induced Unconsciousness. *Anesthesiology, 123*(2), 346-356. doi:10.1097/ALN.0000000000000731

Pandit, J. J., & Cook, T. M. (2013). National Institute for Clinical Excellence guidance on measuring depth of anaesthesia: limitations of EEG-based technology. *Br J Anaesth, 110*(3), 325-328. doi:10.1093/bja/aet006

Perez, W., Dukatz, C., El-Dalati, S., Duncan, J., Abdel-Rasoul, M., Springer, A., Do, M. R., Dzwonczyk, R. (2015). Cerebral oxygenation and processed EEG response to clamping and shunting during carotid endarterectomy under general anesthesia. *J Clin Monit Comput, 29*(6), 713-720. doi:10.1007/s10877-014-9657-4

Purdon, P. L., Pavone, K. J., Akeju, O., Smith, A. C., Sampson, A. L., Lee, J., Zhou, D. W., Solt, K., Brown, E. N. (2015). The Ageing Brain: Age-dependent changes in the electroencephalogram during propofol and sevoflurane general anaesthesia. *Br J Anaesth, 115 Suppl 1*, i46-i57. doi:10.1093/bja/aev213

Purdon, P. L., Sampson, A., Pavone, K. J., & Brown, E. N. (2015). Clinical Electroencephalography for Anesthesiologists: Part I: Background and Basic Signatures. *Anesthesiology, 123*(4), 937-960. doi:10.1097/ALN.0000000000000841

Rampil, I. J. (1998). A primer for EEG signal processing in Anesthesia. *Anesthesiology, 89*, 980-1002.

Rampil, Ira J. (1998). A Primer for EEG Signal Processing in Anesthesia *Anesthesiology, 89*(4), 980-1002. doi:10.1097/00000542-199810000-00023

Ranft, A., Golkowski, D., Kiel, T., Riedl, V., Kohl, P., Rohrer, G., Pientka, J., Berger, S., Thul, A., Maurer, M., Preibisch, C., Zimmer, C., Mashour, G. A., Kochs, E. F., Jordan, D., Ilg, R. (2016). Neural Correlates of Sevoflurane-induced Unconsciousness Identified by Simultaneous Functional Magnetic Resonance Imaging and Electroencephalography. *Anesthesiology, 125*(5), 861-872. doi:10.1097/ALN.0000000000001322

Robinson, A. K., Venkatesh, P., Boring, M. J., Tarr, M. J., Grover, P., & Behrmann, M. (2017). Very high density EEG elucidates spatiotemporal aspects of early visual processing. *Sci Rep, 7*(1), 16248. doi:10.1038/s41598-017-16377-3

Roche-Labarbe, N., Wallois, F., Ponchel, E., Kongolo, G., & Grebe, R. (2007). Coupled oxygenation oscillation measured by NIRS and intermittent cerebral activation on EEG

in premature infants. *Neuroimage, 36*(3), 718-727. doi:10.1016/j.neuroimage.2007.04.002

Rosenthal ES, Biswal S, Zafar SF, et al. Continuous electroencephalography predicts delayed cerebral ischemia after subarachnoid hemorrhage: A prospective study of diagnostic accuracy. Annals of Neurology. 2018 May;83(5):958-969. DOI: 10.1002/ana.25232.

Rubio, A., Hakami, L., Munch, F., Tandler, R., Harig, F., & Weyand, M. (2008). Noninvasive control of adequate cerebral oxygenation during low-flow antegrade selective cerebral perfusion on adults and infants in the aortic arch surgery. *J Card Surg, 23*(5), 474-479. doi:10.1111/j.1540-8191.2008.00644.x

Saidi, N., & Murkin, J. M. (2005). Applied neuromonitoring in cardiac surgery: patient specific management. *Semin Cardiothorac Vasc Anesth, 9*(1), 17-23. doi:10.1177/108925320500900103

Scheeren, T. W. L., Kuizenga, M. H., Maurer, H., Struys, M., & Heringlake, M. (2019). Electroencephalography and Brain Oxygenation Monitoring in the Perioperative Period. *Anesth Analg, 128*(2), 265-277. doi:10.1213/ANE.0000000000002812

Schettler, K. (2013). Das amplitudenintegrierte EEG in der Neonatologie. *Neonatologie Scan, 02*(04), 315-336. doi:10.1055/s-0033-1344907

Schneider, G. J., Dennis; Schwarz, Gerhard. (2014). Monitoring Depth of Anesthesia Utilizing a Combination of Electroencephalographic and Standard Measures. *Anesthesiology, 120*, 819-828.

Schuller PJ, Newell S, Strickland PA, Barry JJ. Response of bispectral index to neuromuscular block in awake volunteers. Br J Anaesth. 2015 Jul;115 Suppl 1:i95-i103. doi: 10.1093/bja/aev072. PMID: 26174308.

Schultz A, G. U., Beger F.A. (2004). The Narcotrend Index Classification Algorithm, Correlation with Propofol Effect-Site Concentrations, and Comparison with Spectral Parameters. *Biomedical Engineering _ Biomedizinische Technik, 49*, 38-42. doi:https://doi-org.eaccess.ub.tum.de/10.1515/BMT.2004.008

Shepherd, J., Jones, J., Frampton, G., Bryant, J., Baxter, L., & Cooper, K. (2013). Clinical effectiveness and cost-effectiveness of depth of anaesthesia monitoring (E-Entropy, Bispectral Index and Narcotrend): a systematic review and economic evaluation. *Health Technol Assess, 17*(34), 1-264. doi:10.3310/hta17340

Slater, J. P., Guarino, T., Stack, J., Vinod, K., Bustami, R. T., Brown, J. M., Rodriguez, A. L., Magovern, C. J., Zaubler, T., Freundlich, K., Parr, G. V. S. (2009). Cerebral Oxygen Desaturation Predicts Cognitive Decline and Longer Hospital Stay After Cardiac Surgery. *The Annals of Thoracic Surgery, 87*(1), 36-45. doi:10.1016/j.athoracsur.2008.08.070

Söhle, M. (2014). Neuromonitoring in der Kardioanästhesie. *Anästh Intensivmed, 55*, 2-19.

Sokol, D. K., Markand, O. N., Daly, E. C., Luerssen, T. G., & Malkoff, M. D. (2000). Near infrared spectroscopy (NIRS) distinguishes seizure types. *Seizure, 9*(5), 323-327. doi:10.1053/seiz.2000.0406

Stein EJ, Glick DB, Minhaj MM, Drum M, Tung A. Relationship between anesthetic depth and venous oxygen saturation during cardiopulmonary bypass. Anesthesiology. 2010 Jul;113(1):35-40. doi: 10.1097/ALN.0b013e3181dc1dfe. PMID: 20508497.Strebel, S., Lam, A. M., Matta, B., Mayberg, T. S., Aaslid, R., & Newell, D. W. (1995). Dynamic and static cerebral autoregulation during isoflurane, desflurane, and propofol anesthesia. *Anesthesiology, 83*(1), 66-76. doi:10.1097/00000542-199507000-00008

Subramanian, B., Nyman, C., Fritock, M., Klinger, R. Y., Sniecinski, R., Roman, P., Huffmyer, J., Parish, M., Yenokyan, G., Hogue, C. W. (2016). A Multicenter Pilot Study Assessing Regional Cerebral Oxygen Desaturation Frequency During Cardiopulmonary Bypass and Responsiveness to an Intervention Algorithm. *Anesth Analg, 122*(6), 1786-1793. doi:10.1213/ANE.0000000000001275

Sun Y, Wei C, Cui V, Xiu M, Wu A. Electroencephalography: Clinical Applications During the Perioperative Period. Front Med (Lausanne). 2020 Jun 9;7:251. doi: 10.3389/fmed.2020.00251. PMID: 32582735; PMCID: PMC7296088.

Suzuki, S., Takasaki, S., Ozaki, T., & Kobayashi, Y. (1999). *Tissue oxygenation monitor using NIR spatially resolved spectroscopy* (Vol. 3597): SPIE. Optical Tomography and Spectroscopy of Tissue III. https://doi.org/10.1117/12.356862

Thudium, M., Heinze, I., Ellerkmann, R. K., & Hilbert, T. (2018). Cerebral Function and Perfusion during Cardiopulmonary Bypass: A Plea for a Multimodal Monitoring Approach. *Heart Surg Forum, 21*(1), E028-E035. doi:10.1532/hsf.1894

Toet, M. C., Lemmers, P. M., van Schelven, L. J., & van Bel, F. (2006). Cerebral oxygenation and electrical activity after birth asphyxia: their relation to outcome. *Pediatrics, 117*(2), 333-339. doi:10.1542/peds.2005-0987

Tovedal, T., Thelin, S., & Lennmyr, F. (2016). Cerebral oxygen saturation during pulsatile and non-pulsatile cardiopulmonary bypass in patients with carotid stenosis. *Perfusion, 31*(1), 72-77. doi:10.1177/0267659115586280

Van Lieshout, J. J., Wieling, W., Karemaker, J. M., & Secher, N. H. (2003). Syncope, cerebral perfusion, and oxygenation. *J Appl Physiol (1985), 94*(3), 833-848. doi:10.1152/japplphysiol.00260.2002

Variane, G. F. T., Chock, V. Y., Netto, A., Pietrobom, R. F. R., & Van Meurs, K. P. (2019). Simultaneous Near-Infrared Spectroscopy (NIRS) and Amplitude-Integrated Electroencephalography (aEEG): Dual Use of Brain Monitoring Techniques Improves Our Understanding of Physiology. *Front Pediatr, 7*, 560. doi:10.3389/fped.2019.00560

Viertiö-Oja, H. (2004). Description of the Entropy algorithm as applied in the Datex-Ohmeda S5 Entropy Module. *Acta Anae Scand, 48*, 154-161.

Viertiö-Oja, H. (2004). Description of the EntropyTM algorithm as applied in the Datex-Ohmeda S/5TM Entropy Module. *ACTA ANAESTHESIOLOGICA SCANDINAVICA, 48*, 154-161.

Wolf, M., Ferrari, M., & Quaresima, V. (2007). Progress of near-infrared spectroscopy and topography for brain and muscle clinical applications. *J Biomed Opt, 12*(6), 062104. doi:10.1117/1.2804899

Zanatta, P., Toffolo, G. M., Sartori, E., Bet, A., Baldanzi, F., Agarwal, N., & Golanov, E. (2013). The human brain pacemaker: Synchronized infra-slow neurovascular coupling in patients undergoing non-pulsatile cardiopulmonary bypass. *Neuroimage, 72*, 10-19. doi:10.1016/j.neuroimage.2013.01.033

Zeller, J. B., Herrmann, M. J., Ehlis, A. C., Polak, T., & Fallgatter, A. J. (2010). Altered parietal brain oxygenation in Alzheimer's disease as assessed with near-infrared spectroscopy. *Am J Geriatr Psychiatry, 18*(5), 433-441. doi:10.1097/JGP.0b013e3181c65821

Zhang, D. D., Hou, X. L., Liu, Y. F., Zhou, C. L., Luo, Y. J., & Ding, H. Y. (2012). The utility of amplitude-integrated EEG and NIRS measurements as indices of hypoxic ischaemia in the newborn pig. *Clinical Neurophysiology, 123*(8), 1668-1675. doi:10.1016/j.clinph.2011.10.051

Zheng, F., Sheinberg, R., Yee, M. S., Ono, M., Zheng, Y., & Hogue, C. W. (2013). Cerebral near-infrared spectroscopy monitoring and neurologic outcomes in adult cardiac surgery patients: a systematic review. *Anesth Analg, 116*(3), 663-676. doi:10.1213/ANE.0b013e318277a255

Appendix

a. List of figures

b. List of tables

c. Supplementary figures

EuroScore II	number of cases	note
1	62	single major cardiac procedure which is not isolated coronary artery bypass grafting
2	99	two major cardiac procedures
3	67	three or more major cardiac procedures
not classified	79	

Weight of analyzed procedures according to EUROScoreII *(referred to 2.1. Data recording).*

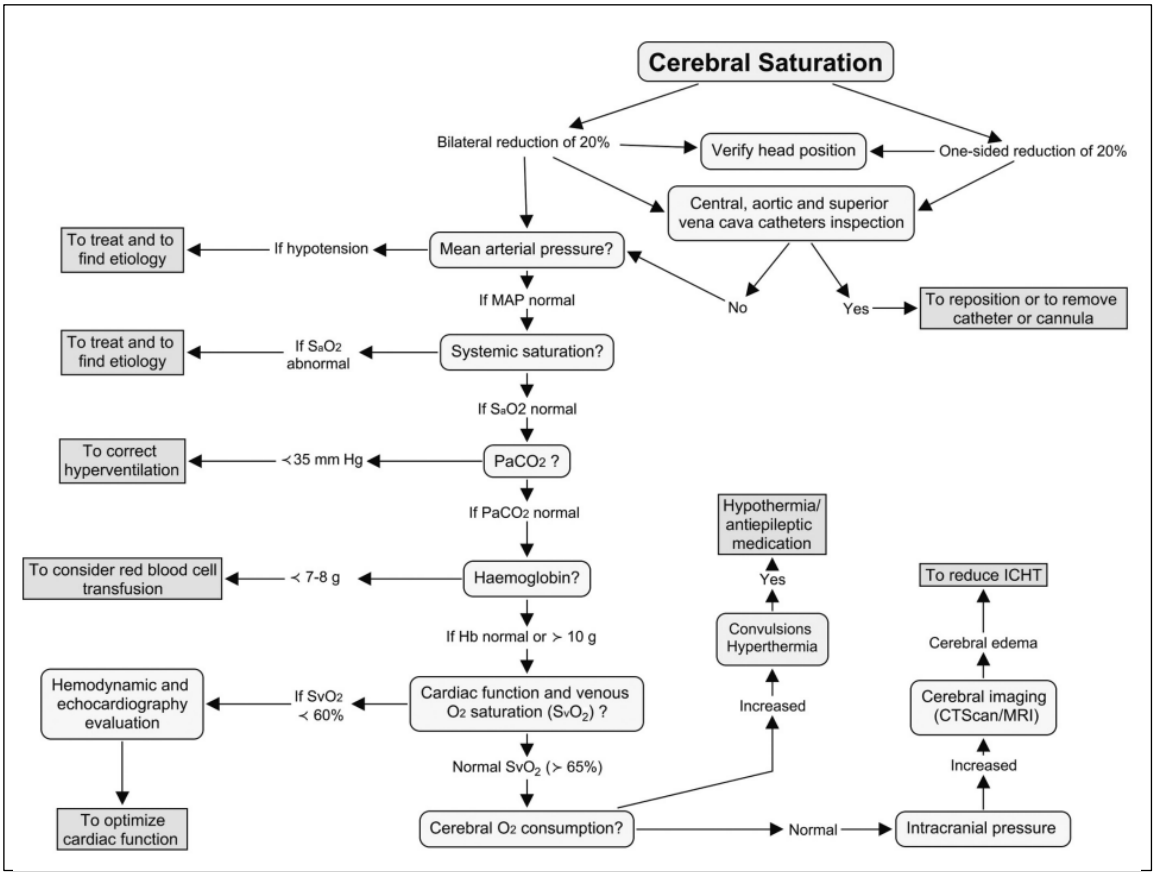

Proposed algorithm in the use of brain oximetry by Denauld et al. (referred to *1.1.2. Development of Near Infrared Spectroscopy).* CT = Computer tomography, ICTH = intracranial hypertension, MAP = mean arterial pressure, MRI = magnetic resonance imaging.

The figures on the following pages present the rEEG, NIRS and aaMAC values (referred to *3.5. Distribution of the range Electroencephalography parameters of the pooled data: 3D-histograms*) on larger scale:

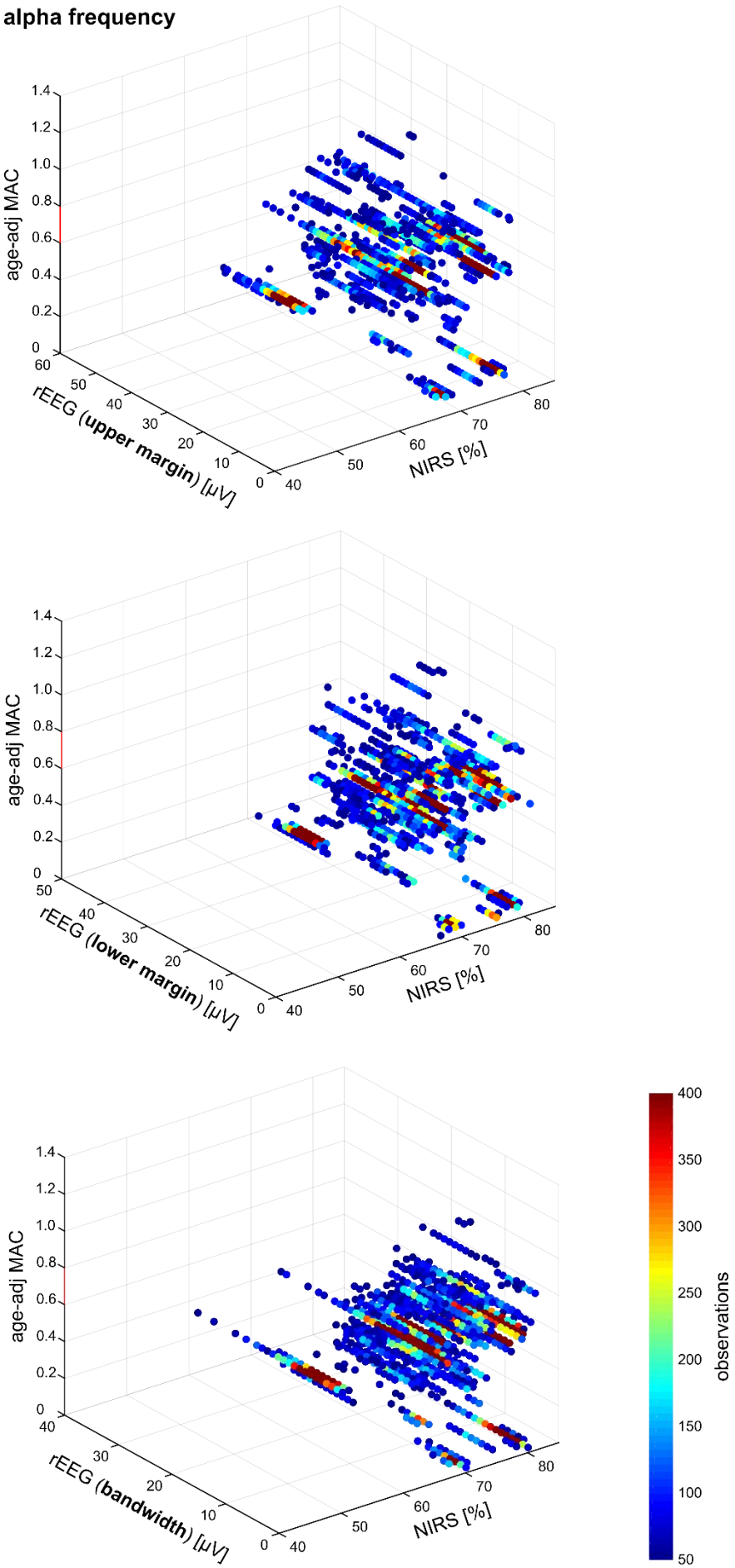
alpha frequency
age-adj MAC
rEEG (upper margin) [µV]
NIRS [%]
rEEG (lower margin) [µV]
rEEG (bandwidth) [µV]
observations

D

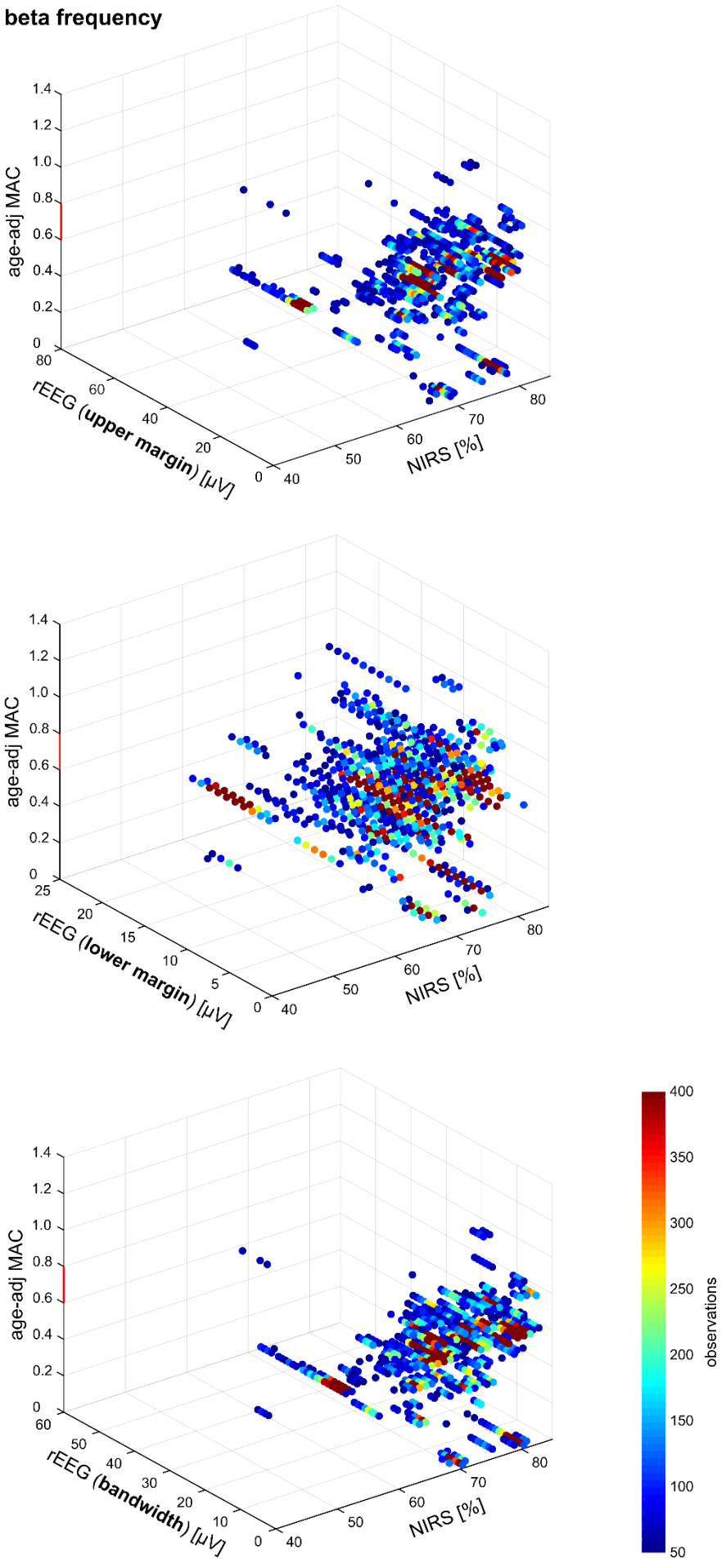
beta frequency
age-adj MAC
rEEG (upper margin) [µV]
NIRS [%]
rEEG (lower margin) [µV]
rEEG (bandwidth) [µV]
observations

E

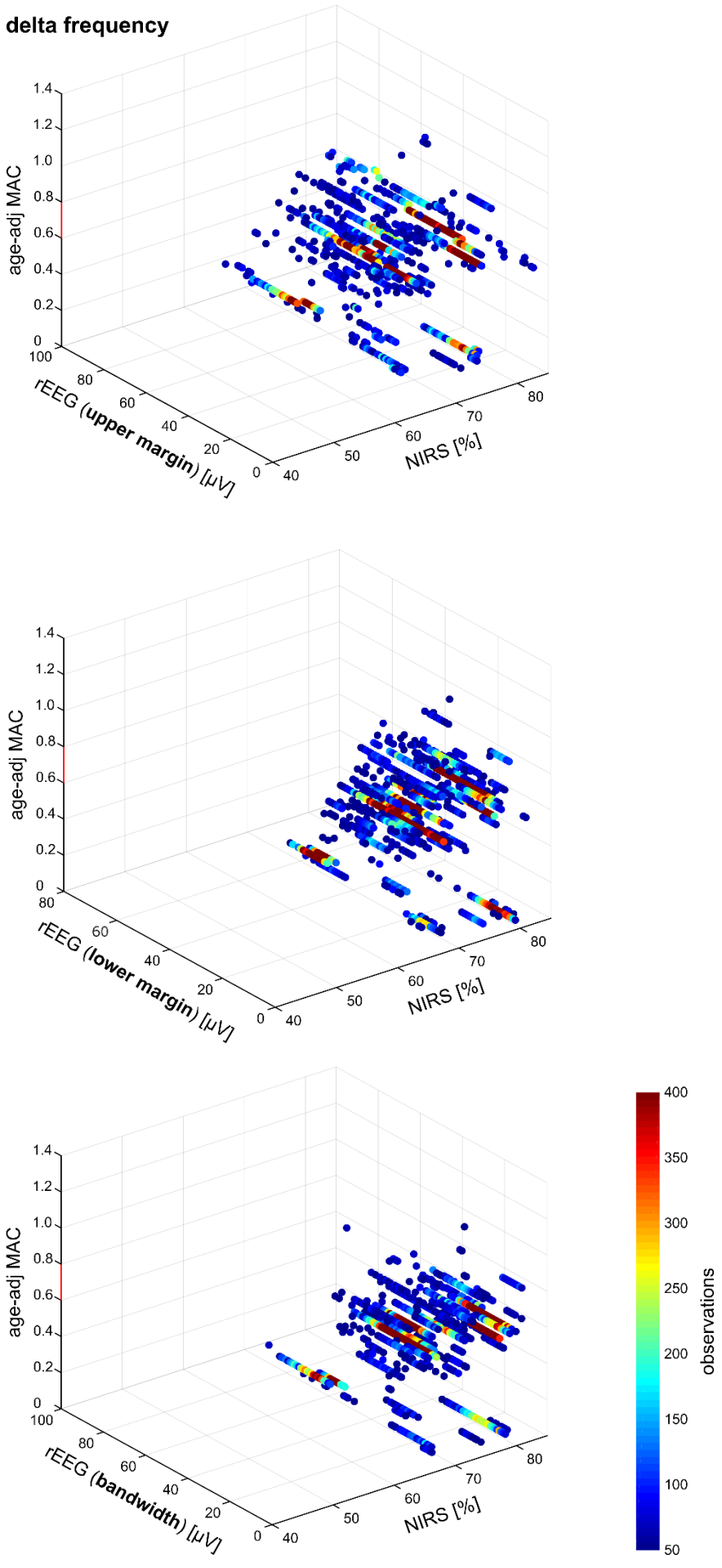
delta frequency
age-adj MAC
rEEG (upper margin) [µV]
NIRS [%]
rEEG (lower margin) [µV]
rEEG (bandwidth) [µV]
observations

F

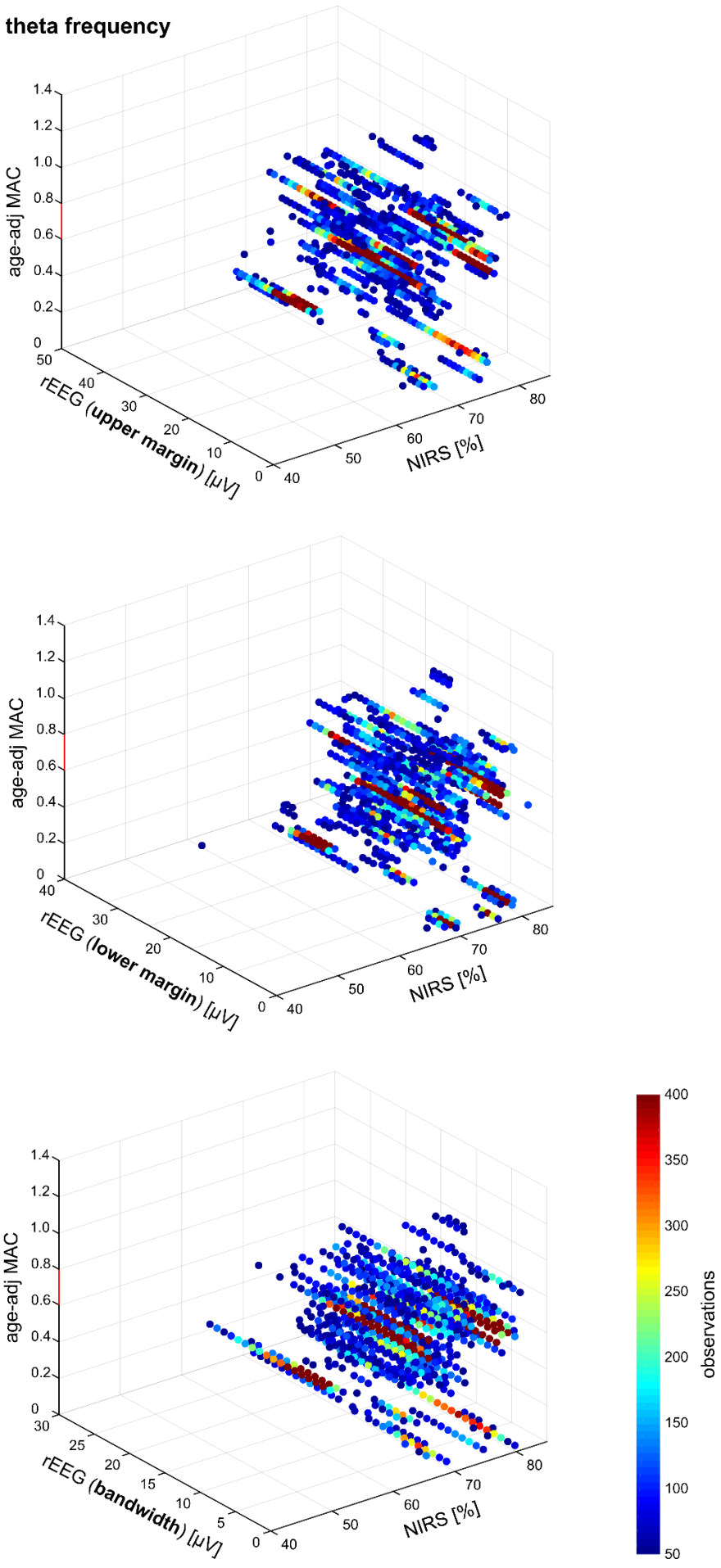
theta frequency
age-adj MAC
rEEG (upper margin) [µV]
NIRS [%]
rEEG (lower margin) [µV]
rEEG (bandwidth) [µV]
observations

G

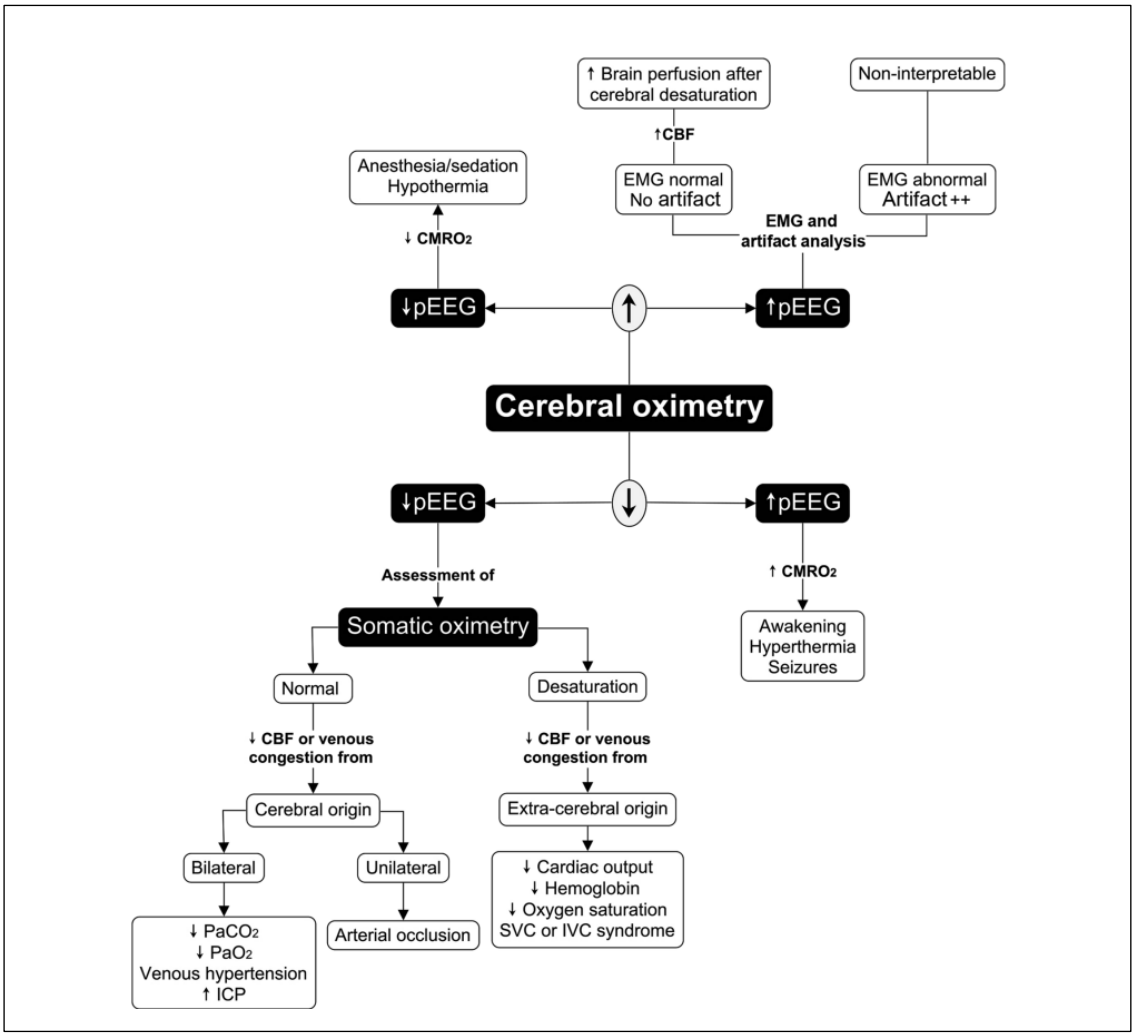

Approach to combined cerebral oximetry monitoring and processed electroencephalography (pEEG) by Couture et al. (referred to *4.2. integration into literary context*).

d. List of equations